The role of secondary cyclones and cyclone families for the North Atlantic storm track and clustering over western Europe

Article

Published Version

Creative Commons: Attribution 4.0 (CC-BY)

Open Access

It is advisable to refer to the publisher's version if you intend to cite from the work. See Guidance on citing.

To link to this article DOI: http://dx.doi.org/10.1002/qj.3733

Publisher: Royal Meteorological Society

the End User Agreement.

www.reading.ac.uk/centaur

CentAUR

Central Archive at the University of Reading

Reading's research outputs online

RESEARCH ARTICLE

The role of secondary cyclones and cyclone families for the North Atlantic storm track and clustering over western Europe

Matthew D. K. Priestley[1] | Helen F. Dacre[1] | Len C. Shaffrey[2] | Sebastian Schemm[3] | Joaquim G. Pinto[4]

[1]Department of Meteorology, University of Reading, Reading, UK

[2]National Centre for Atmospheric Science, Department of Meteorology, University of Reading, Reading, UK

[3]Institute for Atmospheric and Climate Science, ETH Zürich, Zürich, Switzerland

[4]Institute of Meteorology and Climate Research, Karlsruhe Institute of Technology, Karlsruhe, Germany

Correspondence
M. D. K. Priestley, College of Engineering, Mathematics and Physical Sciences, University of Exeter, Exeter, UK.
Email: m.priestley@exeter.ac.uk

Present address
Matthew D. K. Priestley, College of Engineering, Mathematics and Physical Sciences, University of Exeter, Exeter, UK.

Abstract

Secondary cyclones are those that form in association with a pre-existing primary cyclone, typically along a trailing cold front. In previously studied cases they have been shown to cause extreme damage across Europe, particularly when multiple cyclones track over the same location in rapid succession (known as cyclone clustering). To determine the dynamical relationship between primary and secondary cyclones over the North Atlantic, a frontal identification algorithm is partnered with a cyclone identification method to objectively identify secondary cyclones in 35 extended winter periods using reanalysis data. Cyclones are grouped into "cyclone families" consisting of a single primary cyclone and one or more secondary cyclones. This paper aims to quantify the differences between secondary and primary cyclones over the North Atlantic, and how cyclone families contribute to episodes of cyclone clustering across western Europe. Secondary cyclones are shown to occur most frequently in the central and eastern North Atlantic, whereas primary cyclones are commonly found over the western North Atlantic. Cyclone families have their strongest presence over the North Atlantic Ocean and contribute more than 50% of cyclones over the main North Atlantic storm track. A final category, solo cyclones, which are not associated with cyclogenesis on any connected fronts, are most commonly identified over continental regions as well as the Mediterranean Sea. Primary cyclones are associated with the development of an environment that is favourable for secondary cyclone growth. Enhanced Rossby wave breaking following primary cyclone development leads to an increase in the upper-level jet speed and a decrease in low-level stability. Secondary cyclogenesis commonly occurs in this region of anomalously low stability, close to the European continent. During periods of cyclone clustering, secondary cyclones are responsible for approximately 50% of the total number of cyclones. The increase in jet speed

and decrease in static stability initiated by the primary cyclones acts to concentrate the genesis region of secondary cyclones and direct the cyclones that form along a similar track. While there is an increase in the secondary cyclogenesis rate near western Europe during periods of European clustering, the basin-wide secondary cyclogenesis rate decreases during these periods. Thus the large-scale environment redistributes secondary cyclones during periods of clustering rather than increasing the total number of secondary cyclones.

1 | INTRODUCTION

The original conceptual model for extratropical cyclones is the Norwegian model (Bjerknes and Solberg, 1922), which describes how cyclones form and develop throughout their lifetime. The Norwegian model also describes how "cyclone families" can form along the polar front, with each successive cyclone forming slightly to the south and west of the one preceding it. This phenomenon of cyclone families and in particular cyclogenesis along fronts has been studied and observed in previous case studies (e.g., Rivals *et al.*, 1998; Chaboureau and Thorpe, 1999), with the cyclones forming on the trailing fronts of pre-existing cyclones commonly described as "secondary" cyclones.

Secondary cyclones often develop explosively and have a tendency to cause large amounts of damage, as exemplified by the Great Storm of 1987 (Hoskins and Berrisford, 1988), Storms *Lothar* and *Martin* in 1999 (Pearce *et al.*, 2001; Wernli *et al.*, 2002), and Storm *Kyrill* in January 2007 (Ludwig *et al.*, 2015). These secondary cyclones tend to form from frontal-wave instabilities along fronts associated with pre-existing cyclones (often termed "primary" cyclones). However, in some cases (~50%) these frontal-wave instabilities do not develop into cyclones (Parker, 1998), making secondary cyclones difficult to forecast. "Cyclone families" are made up of these primary cyclones and any subsequent secondary cyclones.

Secondary and primary cyclones can differ greatly in terms of their formation mechanisms. The general formation mechanism of primary cyclones is well understood, as these systems commonly form through baroclinic instability that occurs via the interaction of Rossby waves (Hoskins *et al.*, 1985). With regard to the North Atlantic storm track, this cyclogenesis often occurs near the coast of the North American continent and arises from the strong temperature gradients provided by the sea-surface temperature gradient of the Gulf Stream and the contrasting temperatures of the North American continent (Brayshaw *et al.*, 2009; 2011). The formation mechanism of secondary cyclones is more complex, and it has been shown that there are many more processes contributing to wave growth.

The theoretical understanding of frontal-wave growth comes from Joly and Thorpe (1990) and Schär and Davies (1990), who describe how a potential temperature (θ) or potential vorticity (PV) anomaly along a frontal feature can generate frontal instability and hence wave growth. The analytical model of Bishop and Thorpe, (1994a; 1994b) predicted that frontal-wave growth was very unlikely for stretching/deformation rates above $0.6–0.8 \times 10^{-5}$ s^{-1}, something that was later confirmed by Schemm and Sprenger (2015). Dacre and Gray (2006) demonstrated that a relaxation of the frontal strain following the generation of the PV/θ was crucial for the generation of individual frontal waves and summarized the process as follows: a deformation flow along the front drives upward motion which results in latent heat release and forms a PV anomaly strip. This deformation then relaxes, causing a breakdown of the PV strip into smaller anomalies, which may then develop further via interaction with an upper-level wave, this being consistent with Type C cyclogenesis (Plant *et al.*, 2003). This further development of secondary cyclones is not guaranteed (Parker, 1998), with many other contributing factors modulating further growth, including frontal shear (Chaboureau and Thorpe, 1999), latent heat release (Uccellini *et al.*, 1987; Hoskins and Berrisford, 1988; Kuo *et al.*, 1995; Plant *et al.*, 2003), friction in the boundary layer (Adamson *et al.*, 2006) and coastal frontogenesis (Miller, 1946; Bell and Bosart, 1989; Gyakum *et al.*, 1996).

There have been previous attempts to identify secondary cyclogenesis occurring on fronts. The key requirement for identifying these events is the presence of a pre-existing synoptic-scale front. There are two main methods for identifying fronts in gridded meteorological data. The first is a thermodynamic method that uses a low-level thermal gradient (commonly equivalent potential temperature) to identify frontal features. This method is mainly based on the framework presented by Hewson

(1998) and has been used in a number of studies for the purpose of identifying synoptic-scale fronts (Berry *et al.*, 2011; Catto and Pfahl, 2013; Schemm *et al.*, 2018). A second method is based on the directional shift and acceleration of the 10-m wind, as described by Simmonds *et al.* (2012). This method has also been used in other studies (Papritz *et al.*, 2014). The two methods were compared by Hope *et al.* (2014) and Schemm *et al.* (2015). They were found to be consistent by Hope *et al.* (2014), but Schemm *et al.* (2015) found the thermodynamic method to be much better suited to fronts in strongly baroclinic situations (i.e., midlatitude weather systems), with the wind method being better suited to regions of strong convergence or wind shear, as well as to elongated, meridionally oriented fronts.

Schemm and Sprenger (2015) used the thermodynamic method to identify synoptic fronts, and the cyclone identification and tracking methodology of Wernli and Schwierz (2006) to identify the cyclogenesis associated with them. This study found that, in the December, January, February (DJF) period of 35 winter seasons (1979/1980–2013/2014), approximately 8–16% of all cyclogenesis events in the western North Atlantic were secondary cyclone events, and this was slightly lower at 6–10% in the central North Atlantic. Schemm and Sprenger (2015) also showed how secondary cyclones in the eastern North Atlantic were associated with neutral-to-negative anomalies in low-level static stability surrounding the cyclone at the time of genesis, consistent with Wang and Rogers (2001) and Dacre and Gray (2009); however, they did not investigate the evolution of the environment surrounding secondary cyclones prior to or after genesis. A follow-up study by Schemm *et al.* (2018) found that the tracks of secondary cyclones tended to be located more in the central and eastern parts of the North Atlantic ocean (their fig. 5b) and not above the Gulf Stream, as one might expect when considering all cyclones (Hoskins and Hodges, 2002). The identified secondary cyclones in Schemm *et al.* (2018) make up more than 20% of all cyclones in the central and eastern North Atlantic during DJF. Despite the comprehensive analysis of secondary cyclones by Schemm and Sprenger (2015) and Schemm *et al.* (2018), these authors did not objectively identify and compare the related primary cyclones, or quantify any differences in their preferential locations of genesis, track and lysis.

Extratropical cyclones have been shown to cluster across western Europe (Mailier *et al.*, 2006; Vitolo *et al.*, 2009; Pinto *et al.*, 2014; Priestley *et al.*, 2017a; 2017b), a process whereby many more cyclones impact a particular geographical region than one would normally expect. Economou *et al.* (2015) hypothesized that there are three main reasons why extratropical cyclones may

cluster across the North Atlantic: (1) by pure chance; (2) through modulation by large-scale atmospheric patterns, such as the North Atlantic Oscillation (NAO); and (3) through a dependence between successive cyclones (i.e., cyclone families). Mailier *et al.* (2006) and Economou *et al.* (2015) both showed how the phase of the NAO was associated with a large amount of the variability of clustering across the North Atlantic. Walz *et al.* (2018) further highlighted the importance of the NAO phase, but also the East Atlantic (EA) and Scandinavian (SCA) patterns, in playing a role in modulating the interannual variability of serial clustering. The presence of cyclone families during periods of clustering was first highlighted by Pinto *et al.* (2014), as well as in the case study of the 2013/2014 winter season in the UK by Priestley *et al.* (2017a). Both of these periods were accompanied by a strong and zonally extended jet that was flanked by Rossby wave breaking (RWB) on either side, steering intense cyclones and cyclone families downstream towards Europe (see also Hanley and Caballero, 2012; Gómara *et al.*, 2014a; Messori and Caballero, 2015). It is yet to be established what causes the increase in cyclone numbers during periods of clustering and whether secondary cyclogenesis plays a relatively more important role.

In this study, some gaps in the literature presented above are addressed. In particular, the differences between secondary and primary cyclones in the North Atlantic are identified, as well as how secondary cyclones and their associated cyclone families contribute to periods of clustering across western Europe. The questions to be answered are as follows:

1. What is the spatial relationship in the genesis and track density of primary and secondary cyclones in the North Atlantic?
2. How do the upper- and lower-level environments evolve during the formation of primary and secondary cyclones?
3. To what extent do secondary cyclones contribute to the increase in the number of cyclones during periods of clustering that impact western Europe?

This paper is organized as follows. In section 2 the data and methodology used in this study are presented. Following this, results are discussed in section 3. This begins with a climatological discussion of the track, genesis and lysis densities of the different classes of cyclones in section 3.1, with question 1 above addressed in section 3.2. The role of the upper-level environment in cyclogenesis posed by question 2 is then addressed in section 3.3. Finally, a discussion of the role of secondary cyclones in clustering follows in section 3.4, which addresses question 3. In section 4 the key findings are discussed and summarized.

2 | DATA AND METHODOLOGY

2.1 | Dataset

For all of our analysis, the European Centre for Medium-Range Weather Forecasts (ECMWF) ERA-Interim reanalysis is used (Dee *et al.*, 2011). The extended winter period of November, December, January, February (NDJF) from the period 1979/1980–2014/2015 inclusive is used. The horizontal resolution of ERA-Interim is T255 (∼80 km in midlatitudes), with 60 vertical levels and 6-hourly temporal resolution.

2.2 | Cyclone and front identification

To identify and track extratropical cyclones we use the methodology of Murray and Simmonds (1991) that was adapted for Northern Hemisphere cyclones by Pinto *et al.* (2005). Cyclones are identified using the Laplacian of mean sea level pressure (MSLP) ($\nabla^2 p$), which is a proxy for the local geostrophic vorticity. The cyclone location is then identified as the minimum in terms of MSLP that is closest to the maximum in $\nabla^2 p$, in order to relate the identified feature to a "real" low-pressure core. Tracks are filtered to remove weak (maximum $\nabla^2 p > 0.6 hPa$ deg.lat.$^{-2}$), short-lived (cyclone lifetime ≥ 24 hr) and non-developing (maximum $\frac{d}{dt}\nabla^2 p \geq 0.3 hPa$ deg.lat.-2day^{-1}) cyclones based on the criteria from Pinto *et al.* (2009). This method has been shown to compare well to other tracking schemes in terms of individual tracks (Neu *et al.*, 2013) and seasonal track statistics (Pinto *et al.*, 2016), and has been used widely in the scientific literature (e.g., Raible *et al.*, 2008; Flocas *et al.*, 2010; Hofstätter *et al.*, 2016). The track, genesis and lysis density statistics are calculated on a seasonal basis following the method of Hoskins and Hodges (2002). Density statistics are calculated as the number density per month per 5° spherical cap. Track densities are calculated across the whole lifetime of all tracks, with genesis and lysis densities using the first and last time step of each track, respectively.

In order to identify cyclogenesis on synoptic fronts, the fronts themselves must first be identified. To do this, the method of Schemm *et al.* (2015) and Schemm and Sprenger (2015) is followed. This method uses the thermal front parameter and identifies fronts as having a minimum gradient in equivalent potential temperature (θ_e) at 850 hPa of at least 3.5 K per 100 km. Furthermore, all fronts must have a minimum length of 500 km. This ensures that only synoptic-scale features are identified as opposed to weak, baroclinic zones. A further filter is applied to the data so that any frontal features within 2° latitude/longitude of another front are classified as the same feature. This

method for identifying synoptic-scale features has been tested and validated for all types of front in the Northern Hemisphere (Schemm *et al.*, 2015; Schemm and Sprenger, 2015; Schemm *et al.*, 2018). There are other methods that can be used for frontal identification (e.g., Simmonds *et al.*, 2012) and also variants in the method applied in this study by using different thermal front parameters (e.g., θ, Thomas and Schultz, 2019; θ_w, Berry *et al.*, 2011). In Schemm *et al.* (2018) it was shown that the use of θ or θ_e produced consistent results, with θ_e being preferred due to its conservation for moist adiabatic motion and its use in operational frontal identification (Hewson, 1998).

2.3 | Classifying secondary cyclogenesis

To identify cyclogenesis on pre-existing fronts, a similar method to that of Schemm *et al.* (2015) is used. The process described herein is also summarized in the decision tree in Figure 1. In order to identify secondary cyclogenesis, an objectively identified cyclone must first have had its genesis point within 200 km of a frontal feature. This front must also be connected to a pre-existing cyclone in order for the cyclone to be classed as secondary. The front is connected to another cyclone if it is located within 500 km of the cyclone. In situations where there are multiple cyclones within 500 km of a front that all satisfy the criteria of a primary cyclone, only the closest cyclone to the front is taken as the primary cyclone. This ensures that there is a one-to-one correspondence between primary cyclones and secondary cyclones. All cyclones that are classed as secondary, or those that satisfy the criteria for both primary and secondary cyclones (i.e., a secondary cyclone that later in its life becomes the primary cyclone for another secondary cyclone), are then classed as secondary+ cyclones. This ensures that each cyclone family has one primary cyclone associated with it, but potentially multiple secondary+ cyclones. The first cyclone in a family is always classed as the primary cyclone, with any subsequent cyclones in a family being termed secondary+ cyclones. Any cyclones that do not satisfy the criteria of being a primary or a secondary+ cyclone are classed as solo cyclones. Solo cyclones may or may not be associated with fronts at some point in their lifetime; if this is the case, there will be no cyclogenesis occurring along the connected front at any time.

Based on the above methodology, three different types of cyclones are classified.

1. Primary: cyclones associated with a frontal feature at some point during their lifetime, with the front subsequently associated with the cyclogenesis of another cyclone. These are the first cyclones in a cyclone family.
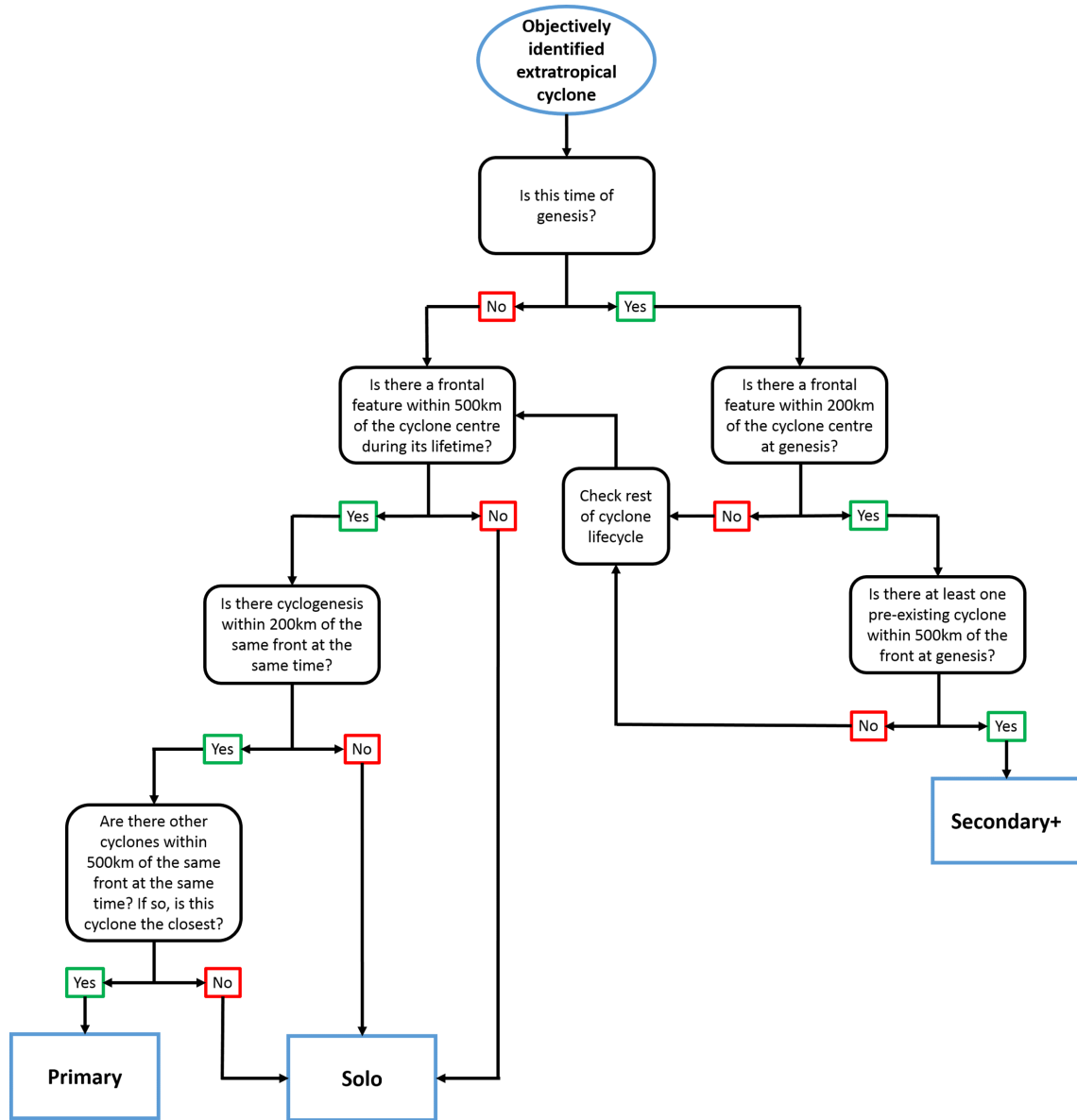
FIGURE 1 A decision tree for classifying the different types of cyclones that make up a cyclone family. Each cyclone can only be classified once

2. Secondary+: cyclones that form within 200 km of a pre-existing front that are in turn associated with a previously identified cyclone. These cyclones are any that are not the first in a cyclone family.

3. Solo: these cyclones may be associated with fronts during their lifetimes, but these fronts are not associated with cyclogenesis along them. Alternatively, they may have no associated frontal features at any point in their lifetime.

In parts of this study, "family" cyclones are also referred to. These cyclones are simply the sum of primary and secondary+ cyclones. For all of the classifications described in this section the methodology is applied to all cyclones in the Northern Hemisphere. In the results section of this study the focus will be solely on the North Atlantic and western Europe and a subset of all the cyclone families identified will be presented. An illustrative example of the method is shown in Figure 2. Sensitivity tests have shown that the number of secondary+ cyclones identified is insensitive to the choice of front search radius from the primary cyclone. The number of secondary+ cyclones identified is sensitive to the 200-km cyclogenesis radius for cyclogenesis occurring along a front; this radius was chosen in order to be consistent with various objective case studies and for similarity with previous work (Schemm and Sprenger, 2015; Schemm *et al.* 2018).
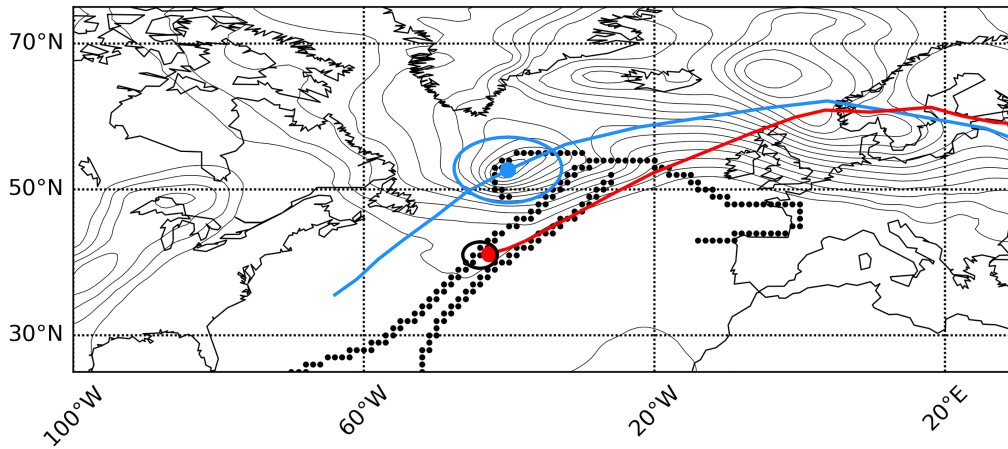
FIGURE 2 An illustrative example of how secondary cyclones and cyclone families are classified from January 11, 2007 at 1800 UTC. The blue line represents the entire cyclone track of a primary cyclone, with the blue dot indicating its location at 1800 UTC on January 11, 2007. The red line is the entire cyclone track of the identified secondary+ cyclone, with the red dot indicating its location at 1800 UTC on January 11, 2007. The blue circle is the 500-km search radius for associating fronts with primary cyclones. The black dots show the location of the connected front at 1800 UTC on January 11, 2007. The black circle indicates the 200-km radius used to search for the cyclogenesis of a secondary+ cyclone associated with the connected front. The light grey contours are mean sea level pressure

2.4 | Large-scale environmental variables

To evaluate the state of the large-scale environment at times of secondary+ cyclogenesis, several variables are investigated. The first is the upper-level jet, which is taken as the 250 hPa wind speed anomaly from the 1979–2015 November–February (NDJF) climatology. Another upper-level feature investigated is that of Rossby wave breaking (RWB). The method of Masato *et al.* (2013) is used to identify regions of RWB on the dynamical tropopause (2-PVU[1] surface: 1 PVU = 1×10^{-6} K m^2 kg^{-1} s^{-1}). RWB is diagnosed as the reversal of the climatological meridional gradient in θ and will be expressed as an anomaly of the frequency of RWB in a particular location relative to the local climatological frequency (i.e., a frequency of 0.33 in a location where the climatology is 0.3 would have an anomaly value of 0.1, or 10%).

Furthermore, the environment of the lower atmosphere is investigated, specifically the low-level static stability (800–950 hPa averaged). The Brunt–Väisälä frequency (N^2), formulated in pressure (p) coordinates, is calculated and expressed as a relative anomaly to the NDJF climatology. The formulation for N^2 used is shown in Equation 1 and is the local change of θ with pressure (p) that is also scaled by gravity (g), the mean layer temperature (T) and the specific gas constant (R):

$$N^2 = -\frac{pg^2}{RT\overline{\theta}}\frac{\partial\theta}{\partial p}. \tag{1}$$

[1] PVU = potential vorticity unit.

3 | RESULTS

3.1 | Climatology of primary, secondary+ and solo cyclones

Applying the identification criteria laid out in section 2.3 to 36 extended winters, an assessment of the properties of the different types of cyclones is conducted. Figure 3a shows the total NDJF track density of all cyclones and has a characteristic southwest–northeast tilt that extends from the eastern coast of North America towards the coast of Norway and the Nordic Seas. There is a maximum in the density of cyclone tracks in the region between the tip of Greenland and western Iceland, with values of up to 20 cyclones per month. A further maximum in the track density is identified across the central Mediterranean with a maximum of 10–13 cyclones per month downstream of the Gulf of Genoa.

The primary cyclone class track density is shown in Figure 3b. The mean spatial features of Figure 3b are similar to those of Figure 3a. For example, there is a characteristic southwest–northeast tilt in the North Atlantic, but the tracks are now concentrated closer to the east coast of North America, with values of approximately 3–4 cyclones per month in this region. Primary cyclones do not travel as far to the northeast as those shown in Figure 3a, with relatively lower track densities beyond 20°W.

The track density of the secondary+ cyclone class is shown in Figure 3c. Again a southwest–northeast tilt is observed as in Figure 3a,b. However, for secondary+ cyclones the maximum in the track density covers a broader region of the North Atlantic (from approx.
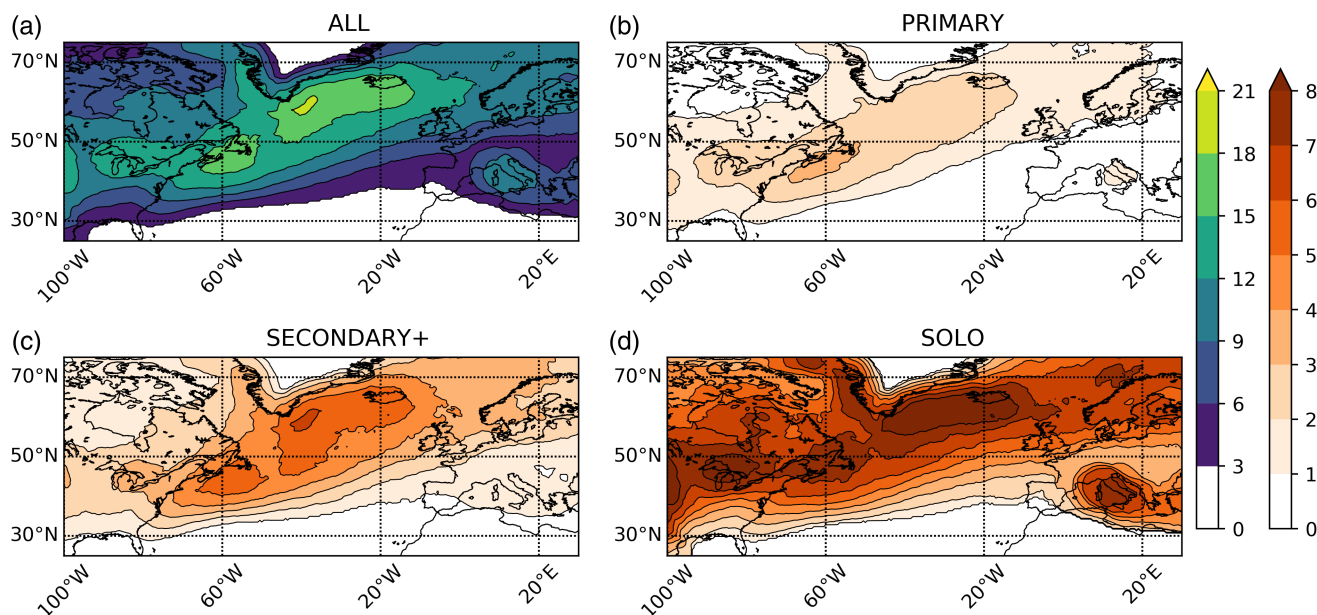
FIGURE 3 Track densities of (a) all cyclones, (b) primary cyclones, (c) secondary+ cyclones and (d) solo cyclones. The unit of density is number of cyclones per month per 5° spherical cap. The lowest contour intervals are not coloured and regions with less than three cyclones per month^{-1} per 5° spherical cap are masked out

40–10°W), with values of 5–7 cyclones per month. This suggests a difference in the preferential geographical location of primary versus secondary+ cyclones in terms of the overall North Atlantic storm track. The secondary+ cyclones may be found further east than primary cyclones on account of primary cyclones having to propagate some way downstream before the genesis of the secondary+ cyclones can occur, as observed by Schemm *et al.* (2018).

The final cyclone class is that of solo cyclones (Figure 3d). Solo cyclones exhibit different mean locations in track density than the primary and secondary+ classes. Firstly, the characteristic southwest–northeast tilt of the track density is less pronounced. The largest densities are not solely confined to the ocean basin as they are for primary and secondary+ cyclones, with a relatively large number of tracks present over the North American continent. The largest densities are in a zonal band between the tip of Greenland and Iceland. The final dominant region for solo cyclones is the Mediterranean (more than seven cyclones per month), which is a large increase compared with the other classes.

The relative contribution of the different cyclone classes to the total track density is shown in Figure 4. Primary cyclones are more prevalent in the western North Atlantic (Figure 4a) and over the eastern coast of North America. They are dominant in the entrance region of the North Atlantic storm track where they make up 20–30% of all cyclones.

Conversely, secondary+ cyclones (Figure 4b) have their largest contribution to the storm track across the

central and eastern North Atlantic and extending northeast towards the Nordic Seas. They make up 40–50% of all cyclones in the central North Atlantic and 30–40% of all cyclones across most of the rest of the North Atlantic Basin and northwestern Europe. This pattern is to some extent similar to the findings from Schemm *et al.* (2018) (their fig. 5b); however, they found that cyclones forming on a trailing front made up 20–30% of all cyclones in the central/eastern North Atlantic. These differences are likely due to the differences in track densities between the cyclone identification method of Pinto *et al.* (2005) applied in this study and the method of Wernli and Schwierz (2006) used by Schemm *et al.* (2018) in this region. Large differences in the track densities can be seen (Pinto *et al.*, 2016; their fig. 2) with up to twice as many cyclones per season in some parts of the equatorward central North Atlantic.

Grouping these two classes together results in the family class (Figure 4d). This illustrates how family cyclones are most dominant in the main storm track region (Figure 3a) and contribute up to 60% of all storms in the North Atlantic. The family cyclones are strongly linked to the oceanic regions, with minimum values over continental regions, and are most prevalent across what one might consider to be the wintertime North Atlantic storm track.

Solo cyclones dominate different locations to family cyclones. The relative contributions of solo cyclones to the total density of cyclones (Figure 4c) are found in North America, specifically northern Canada, and the Mediterranean Sea. In both these regions solo cyclones make up >70% of all cyclones. Solo cyclones are by definition the
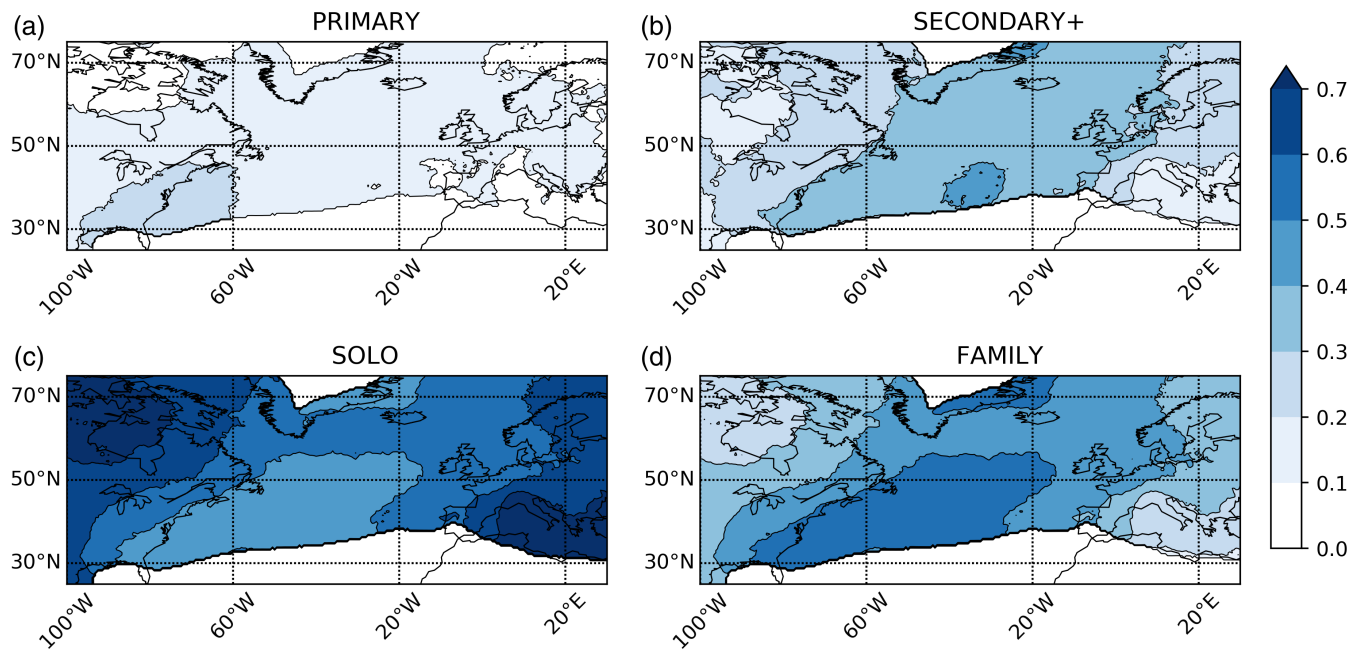
FIGURE 4 Fractional track densities for each cyclone class compared to the overall track densities for (a) primary, (b) secondary+, (c) solo and (d) family (primary and secondary+) cyclones. Regions where the total track density is less than three cyclones per month are masked out

opposite of family cyclones and represent a smaller fraction of the total number of cyclone tracks across the North Atlantic (<50% of all cyclones across most of this region).

Further insight into the differences between the different cyclone classes can be inferred from an examination of their genesis density climatologies (Figure 5). One of the main genesis locations for all cyclones (Figure 5a) is close to the eastern coast of North America and over the Gulf Stream. This is to be expected as the quasi-permanent temperature gradient in this location generates baroclinic instability, which is the dominant driver of midlatitude cyclone formation. Other main regions for cyclogenesis are surrounding the tip of Greenland, over the Gulf of Genoa and downstream of the Rocky Mountains.

For primary cyclones (Figure 5b), the dominant cyclogenesis region is over the Gulf Stream. There are also primary cyclones that form near the tip of Greenland and over the Mediterranean, but with fewer cyclones forming per month than over the Gulf Stream. Unlike primary cyclones, secondary+ cyclones (Figure 5c) have a tendency to form in the central North Atlantic. There is also a substantial amount of secondary+ cyclogenesis near the coast of North America, which may be related to processes such as coastal frontogenesis (Bosart, 1975; Nielsen, 1989; Gyakum *et al.*, 1996) or cold air damming. This difference in the genesis density of secondary+ and primary cyclones, with secondary+ cyclones tending to form further downstream, can be understood as follows. Any primary cyclone that forms over the Gulf Stream then

propagates in a southwest–northeasterly direction with the subsequent secondary+ cyclone then forming on a trailing front, which is likely to be downstream of the Gulf Stream.

The solo cyclone class (Figure 5d) has some cyclogenesis near the coast of North America and the western North Atlantic; unlike for the other classes, however, this is not the dominant region. The main regions are the Mediterranean, the lee side of the Rocky Mountains (not shown) and surrounding the tip of Greenland. Given the mean location of solo cyclogenesis it is possible that solo cyclones are quite different from family cyclones and could be more heavily influenced by processes such as lee cyclogenesis.

The lysis densities of the different cyclone classes have also been investigated as part of this study. The lysis is shown in Figure S1 in the Supplementary Information. The characteristics for the primary and secondary+ cyclone classes are very similar and both tend to have their lysis in the region between Greenland and Iceland and over the North Atlantic (this is consistent with the lysis for all cyclones; Figure S1b,c). Solo cyclones tend to have their lysis across the Mediterranean, and also over parts of North America and the region between Greenland and Iceland (Figure S1d).

3.2 | Structure of a cyclone family

To examine the temporal and spatial relationships between primary and secondary+ cyclones, specific secondary+
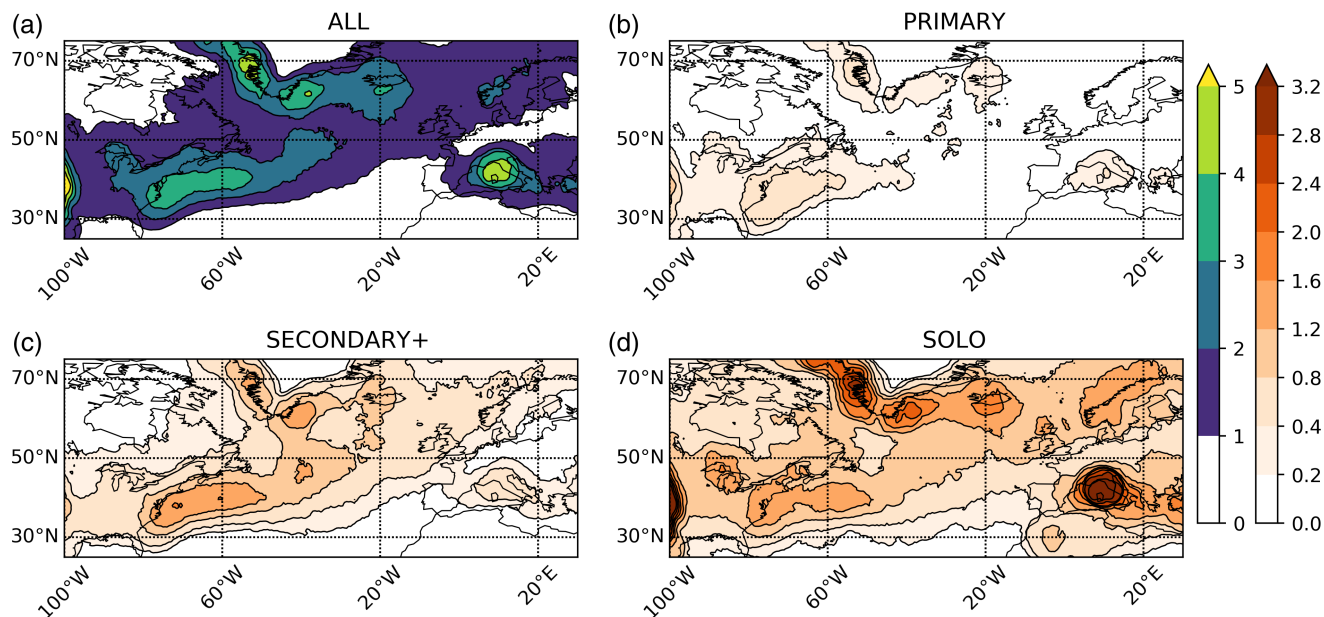
FIGURE 5   Genesis densities of (a) all cyclones, (b) primary cyclones, (c) secondary+ cyclones and (d) solo cyclones. The unit of density is the number of cyclones per month per 5° spherical cap. The lowest contour intervals are not coloured

cyclone events are examined. To select these events, only those cyclones that track through a 700-km radius centred at 55°N, 5°W are included (black dashed region in Figure 6a). This area selection is consistent with Priestley *et al.* (2017b) and allows us to focus on cyclones that affect specific regions of western Europe.
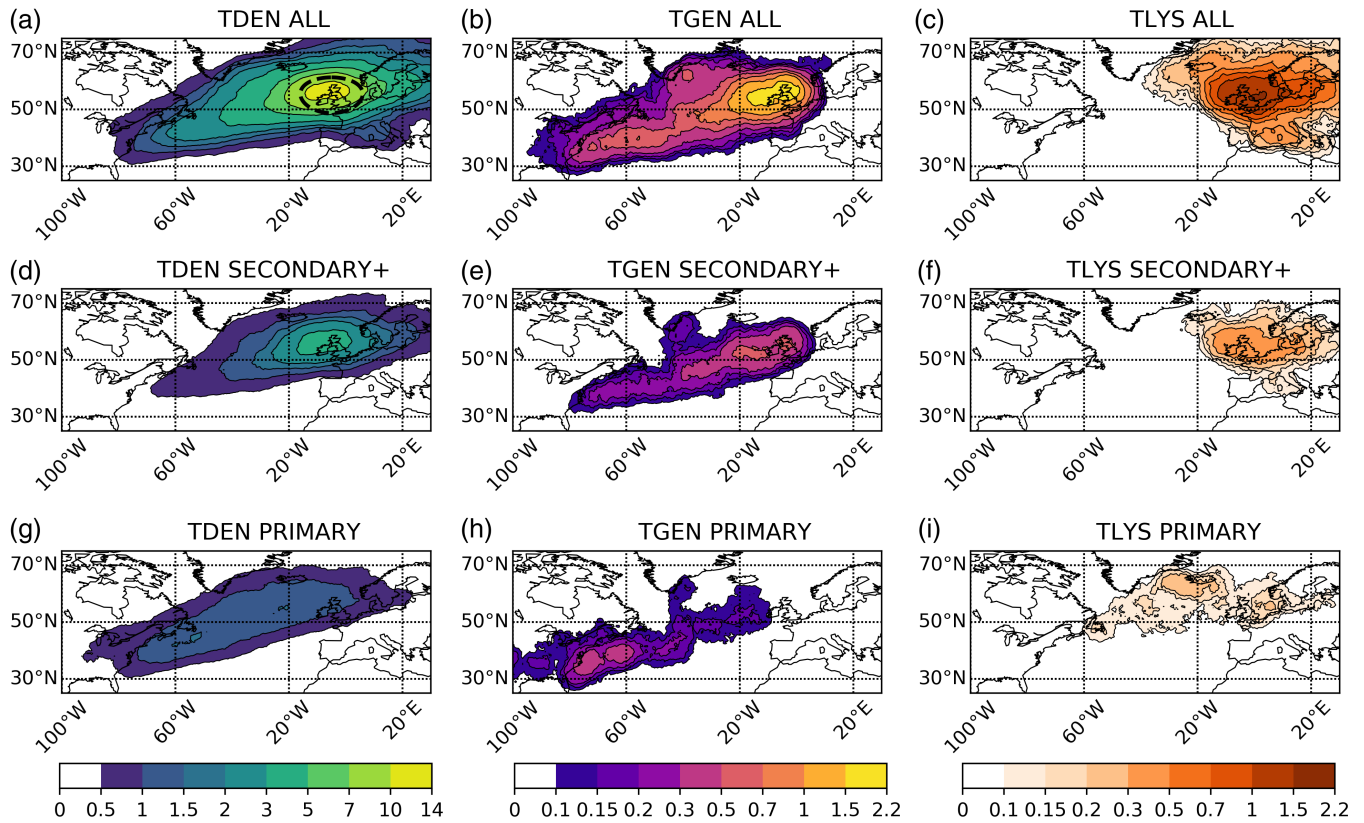
For all storms that pass through the 55°N region, the track density (Figure 6a) is of a more zonal orientation than the total storm track (Figure 3a). Most cyclones are located between 50–60°N and east of 40°W. This is further apparent when looking at the genesis of these cyclones (Figure 6b), as most of the cyclones that pass through 55°N form very close to this region (east of 20°W). The average lysis of these cyclones (Figure 6c) is to the east of the UK, mainly extending further east towards Denmark and across northern Europe. This suggests that the majority of cyclones that track over the UK are short-lived features that form close to the European continent, propagate eastwards in a zonal direction and dissipate shortly afterwards (consistent with Dacre and Gray, 2009).

Similar density patterns are found when investigating the secondary+ cyclones that pass through 55°N (Figure 6d–f). These cyclones also form close to the UK and Europe (Figure 6e), although, as shown in Figure 6b, there are also cyclones that form over the western North Atlantic. The pattern of track density (Figure 6d) is more zonal than the total track density for all storms (Figure 3a), and lysis occurs to the east of the UK over the North Sea and surrounding countries.

A different picture emerges when looking at the density pattern for the primary cyclones that are in the same

family and hence precede the secondary+ cyclones analysed in Figure 6d–f. Unlike the secondary+ cyclones, which are constrained to pass through the 55°N region (Figure 6d–f), the primary cyclones of each family do not have this requirement. The average track density for these primary cyclones (Figure 6g) is different to those shown in Figure 6a,d. The primary cyclones exhibit the southwest–northeast tilt as seen in Figure 3b, with maxima in the cyclone track density near the coast of North America and to the south of Iceland. It is interesting to note that the track density of primary cyclones (Figure 6g) and the genesis density of secondary+ cyclones (Figure 6e) exhibit a similar tilt, with the secondary+ genesis density at a more southerly latitude across the North Atlantic. A majority of the primary cyclones have their genesis over the strong baroclinic zone off the east coast of North America (Figure 6h), unlike the genesis locations of the secondary+ cyclones further downstream. Finally, the lysis locations (Figure 6i) for primary cyclones are in the region between the tip of Greenland and Iceland. This suggests that these primary cyclones do not travel towards the European continent and are mainly constrained to longitudes west of 20°W. The similarity in the lysis longitude of the primary cyclones (Figure 6i) and the genesis of the secondary+ cyclones (Figure 6e) goes some way to confirming the hypothesis of Dacre and Gray (2009) that eastern North Atlantic cyclones are commonly secondary+ cyclones.

In summary, the primary cyclone tends to form over the Gulf Stream or near the coast of North America before travelling in a northeasterly direction across the North Atlantic. These cyclones then have their lysis to the east

FIGURE 6 Density plots for all cyclones (a)–(c), secondary+ cyclones (d)–(f) and the associated primary cyclone of the secondary+ cyclones (g)–(i) that pass through the 55°N region. (a,d,g) Track densities. (b,e,h) Genesis densities. (c,f,i) Lysis densities. The lowest contour intervals are not coloured. The unit of density is the number of cyclones per month per 5° spherical cap. The black dashed region in (a) represents the 700-km region that cyclones must pass through

of Greenland, near Iceland. During their lifetime cyclogenesis occurs along an associated frontal feature, which is generally located in the central-to-eastern North Atlantic, at latitudes of 50–60°N and to the south of the primary cyclone. These secondary+ cyclones then propagate in a much more zonal direction across the UK, before dissipating over the UK or over the North Sea and surrounding countries. This illustrates how the different cyclone classes tend to be preferentially located in different parts of the North Atlantic and the North Atlantic storm track (as suggested in Figure 4). The results of Figure 6 further highlight the misleading nature of mean track densities, as noted by Whittaker and Horn (1984), due to the fact that cyclones rarely travel the length of the entire storm track and the mean storm track is made up of several different types of cyclone.

This analysis was also performed for secondary+ cyclones that pass through two other geographical regions of western Europe at 45°N, 5°W and 65°N, 5°W, as defined in Priestley *et al.* (2017b), and their preceding primary cyclones, which do not have to pass through the specified regions (see Figures S2 and S3). The results of this analysis were very similar to those presented in Figure 6, with the

main difference being a northward/southward shift in the genesis/lysis latitude of the secondary+ cyclones, dependent on the latitude of interest. With this, there are only very minor shifts in the angle of the primary cyclone mean track density. There are clear differences between the primary cyclones and the secondary+ cyclones for all latitude subsets, with primary cyclones having a more poleward element to their track than the secondary+ cyclones that follow them. However, it is interesting to note that despite there being large differences in the latitude of secondary+ cyclogenesis, the tracks of the primary cyclones that precede them are very similar.

3.3 | Large-scale environmental conditions at the time of primary and secondary+ cyclogenesis

3.3.1 | Upper-level jet and Rossby wave breaking

As illustrated in Figure 6, the secondary+ cyclones that pass through 55°N and their respective primary cyclones
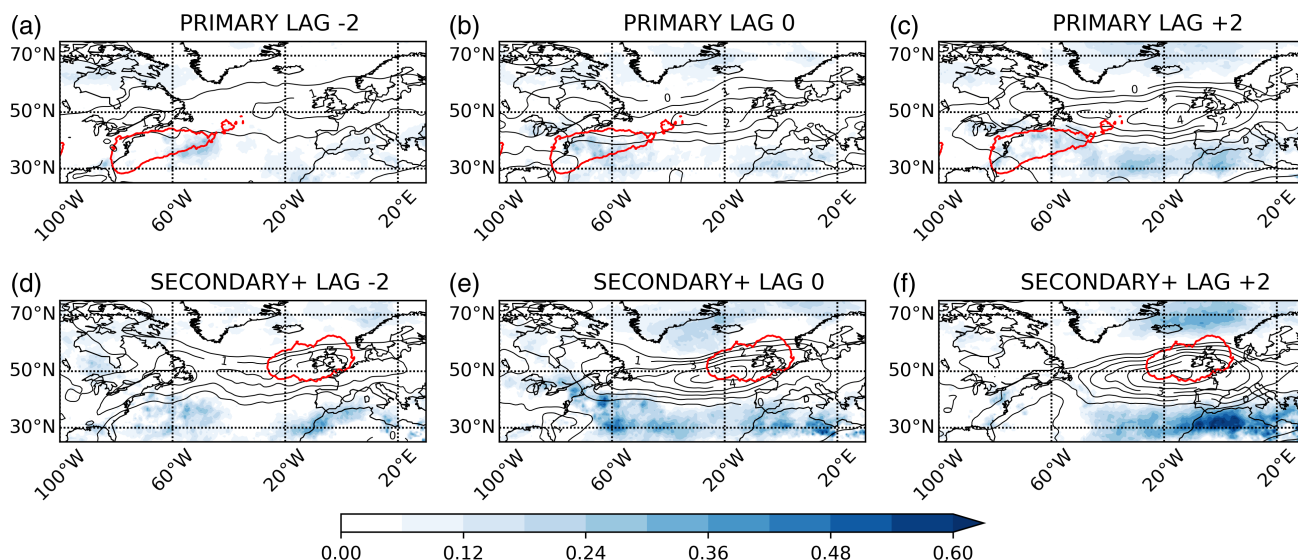
FIGURE 7 Composites of Rossby wave breaking (RWB) and the upper-level jet for secondary+ cyclones that pass through the 55°N region and their respective primary cyclones. Composites are shown at times of (b) primary cyclogenesis and (e) secondary+ cyclogenesis. Also shown are composites at lag −2 days (a,d) and lag +2 days (c,f). Red contours in (a–c) are contours of primary cyclogenesis (at lag 0 days), which is 50% of the maximum value. Red contours in (d–f) are the same as in (a–c) but for secondary+ cyclones. RWB is expressed as an anomaly in the frequency of RWB at that location relative to the local climatological frequency and is shown by the blue shading. Each contour interval is a 6% increase in the frequency. The upper-level jet is illustrated by the black contours as an anomaly in the 250 hPa wind field to the local climatology in m s^{-1} with contours every 1 m s^{-1} above 1 m s^{-1}

form in different locations and are also likely to form under different environmental conditions. To understand any differences, the upper-level features that are associated with these cyclones at their time of genesis is analysed (Figure 7). As has been established in several studies, cyclones that impact western Europe are commonly associated with an anomalously strong upper-level jet and RWB on one or both sides of the jet (Hanley and Caballero, 2012; Pinto *et al.*, 2014; Gómara *et al.*, 2014a; Messori and Caballero, 2015; Priestley *et al.*, 2017b); therefore the same fields will be analysed herein.

We first focus on the time of cyclogenesis for secondary+ cyclones passing through our 55°N region (Figure 7e) and the cyclogenesis time of their respective primary cyclones (Figure 7b). These will be referred to as lag 0 days. For the primary cyclones (Figure 7b), it is seen that anomalies in the upper-level jet and RWB frequency are very small. Jet anomalies are less than 3 m s^{-1}, with RWB frequency anomalies generally less than 10%, with some localized regions ~20% above the climatological frequency. The cyclones are mostly all forming off the east coast of North America, near the right entrance of the jet, and the environment at this time can for the most part be described as climatological, with minor positive anomalies.

At the time of secondary+ cyclone genesis (Figure 7e), the upper-level environment is very different. There are anomalies in the upper-level jet of over 5 m s^{-1} and

anomalous RWB frequencies of up to 40% above the climatological frequency. Both fields have increased anomalies compared to the time of cyclogenesis of the primary cyclones. This environment is representative of the one described in the aforementioned studies (Pinto *et al.*, 2014; Priestley *et al.*, 2017b), with anomalous RWB either side of a zonally extended and strong jet being favourable for the formation and presence of intense cyclones in the eastern North Atlantic. At the time of cyclogenesis, the secondary+ cyclones are forming either on the jet axis or the left exit region of the jet, which suggests that conditions are favourable for cyclogenesis via upper-level divergence provided by ageostrophic circulations in the left exit region of the jet (Rivière and Joly, 2006a; 2006b).

Through inspection of the lag plots, further insight is gained into the connection between the primary and secondary+ cyclones. At lag 2 days after primary cyclone formation (Figure 7c) there is an amplification of the anomalies from lag 0 (Figure 7b) downstream of cyclogenesis and around Iceland and the Nordic Seas. These anomalies are associated with the presence of the primary cyclone in this region, as it is likely to have propagated towards the northeast from its genesis region. The presence of the primary cyclone is associated with the development of anomalous RWB, which then in turn causes an acceleration in the jet (see Priestley *et al.*, 2017b, their fig. 3) through the convergence of eddy momentum (Barnes and Hartmann, 2012). The state of the environment in

Figure 7c is similar to that at secondary+ cyclogenesis time (Figure 7e), albeit with slightly reduced RWB anomalies, suggesting that the primary cyclone might be key in creating an upper-level environment that is favourable for the formation of secondary+ cyclones. Further evidence for this is provided in Figure 7d. Two days prior to secondary+ cyclogenesis, the upper-level environment has very small anomalies in RWB and the jet, which is very similar to that of Figure 7b, and the anomalies are almost zero 2 days prior to primary cyclogenesis (Figure 7a), suggesting that the anomalies are associated with the development and propagation of the primary cyclone in the days prior to secondary+ cyclogenesis. Anomalies are then amplified to an even greater extent as the secondary+ cyclone develops and moves downstream (Figure 7f), with anomalies of RWB more than 60% above the climatology and a very anomalous jet at 250 hPa ($> 6 \text{ m s}^{-1}$).

As for Figure 6, this analysis of Figure 7 is repeated for secondary+ cyclones passing through two other geographical regions at 45°N and 65°N and their preceding primary cyclones (Figures S4 and S5). Similar results to those presented in Figure 7 are found, but with a different balance of the RWB, being more dominant on either the northern or the southern flank, and hence a shift in the latitude of the jet anomalies for cyclones impacting 45°N (Figure S4) and 65°N (Figure S5), respectively, as seen in Priestley *et al.* (2017b). These differences in RWB and primary cyclone genesis/lysis could be interpreted through the two different baroclinic life cycles (LC1/LC2), as first discussed by Thorncroft *et al.* (1993). Primary cyclones that spawn the 65°N secondary+ cyclones may more closely resemble the LC1 life cycle. The primary cyclone appears to form under more anticyclonic shear (Figure S5b). LC1 cyclones are associated with anticyclonic RWB on the equatorward flank of the jet and a northward displacement of the jet, which is similar to what is seen in Figure S5. The lysis of these 65°N primary cyclones (see Figure 9a) also occurs close to the jet axis, with part of the life cycle even being on the equatorward side of the anomalous jet, further suggesting that this could be propagating under the LC1 life cycle. Conversely, the 45°N primary cyclones appear to form under relatively neutral/cyclonic shear (Figure S4b). The LC2 life cycle results in a large amount of cyclonic RWB and a southward displacement of the jet, as is suggested in Figure S4. The lysis of the 45°N cyclones also occurs quite far from the jet axis (Figure 9c), indicating that these primary cyclones may more closely resemble the LC2 life cycle. These results suggest that the environment surrounding the primary cyclone at the time of genesis is associated with differing life cycles and RWB structures downstream, thus affecting the latitude of secondary+ cyclogenesis and the latitude of propagation over western Europe.
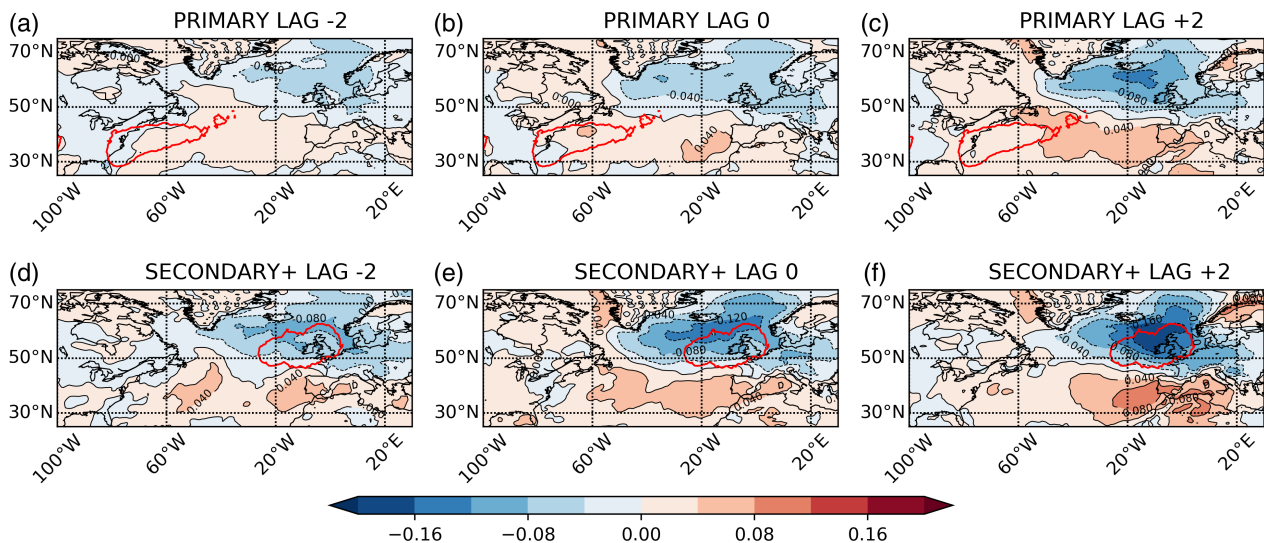
3.3.2 | Low-level static stability

As cyclones forming in the eastern North Atlantic are associated with a low-stability environment (Wang and Rogers, 2001; Dacre and Gray, 2009) and secondary+ cyclones are also associated with reduced low-level stability anomalies (Schemm *et al.*, 2015), the evolution of the low-level stability field at the time of secondary+ cyclogenesis will be investigated. Their respective primary cyclones will also be analysed.

At the time of cyclogenesis (lag 0 days) for the primary cyclone (Figure 8b) there are minimal anomalies (<5%) in static stability across the North Atlantic, with some indication of a north–south dipole between 0 and 20°W, across 50°N. In the region of primary cyclone formation, anomalies are very weak and do not exceed $\pm 4\%$. This process is likely not influenced by the stability, as it is common for cyclones forming in this region to be Type B cyclones (Gray and Dacre, 2006) driven by an upper-level feature interacting with quasi-persistent temperature gradients (Petterssen *et al.*, 1955; Davis and Emanuel, 1991).

Conversely, at the time of secondary+ cyclone formation (Figure 8e), the dipole in anomalous N^2 is much larger, with anomalies more than 12% lower than the local climatology in the northeastern North Atlantic, and more negative on average than the anomalies in the region of primary cyclogenesis. It is in this region of lower N^2 that the secondary+ cyclones are forming. Cyclogenesis in low N^2 environments of the eastern North Atlantic has previously been studied (Wang and Rogers, 2001; Dacre and Gray, 2009), but it is interesting to note that, as with the jet and RWB anomalies in Figure 7, the negative anomalies in N^2 shown in Figure 8 are much stronger at the time of secondary+ cyclogenesis than they are for primary cyclogenesis. As the secondary+ cyclones are forming in a strongly anomalous low N^2 region, it appears that this low stability is important for secondary+ cyclones to form.

As for Figure 7, an amplification of the anomalies associated with the primary cyclones from lag 0 days to lag 2 days is seen (Figure 8b,c), as well as an increase in the anomalies from lag −2 days to lag 0 days for secondary+ cyclogenesis (Figure 8d,e). This increase in the anomaly magnitude is again likely associated with the propagation of the primary cyclone downstream and in a northeasterly direction over a period of approximately 2 days. This amplification of the anomalies in N^2 can be understood through interpretation of the thermal wind balance equation. The acceleration of the jet shown in Figure 7 has an increasing magnitude with height from the surface to the tropopause. Through thermal wind balance there is an associated increase in the meridional temperature gradient near the surface at the time of secondary+ cyclogenesis (not shown). This increase in the meridional temperature

FIGURE 8 Composites of low-level static stability (N^2) for secondary+ cyclones that pass through the 55°N region and their respective primary cyclones are indicated by coloured shading. Composites are shown at times of primary cyclogenesis (b) and secondary+ cyclogenesis (e). Also shown are composites at lag −2 days (a,d) and lag +2 days (c,f). Red contours in (a–c) are contours of primary cyclogenesis (at lag 0 days), which is 50% of the maximum value. Red countours in (d–f) are the same as for (a–c) but for secondary+ cyclones. Anomalies are expressed as percentage changes relative to the local climatology

gradient below the jet axis is expected due to the formation of secondary+ cyclones along a nearby frontal feature. With the increase of the meridional temperature gradient there is also an increase of the vertical potential temperature gradient. This is associated with an increase in the meridional gradient of static stability. Therefore, as the primary cyclone propagates northeastward, it is associated with an increase in RWB and hence an acceleration of the jet. This jet speed increase is then associated with an enhanced temperature gradient across the jet axis and a stronger stability dipole. This results in stability minima at low levels on the northern flank of the jet. This anomalously low stability environment is then conducive to the formation and intensification of secondary+ cyclones in this region. This environmental development is associated with the downstream propagation, development and presence of the primary cyclone in the 2–3 days prior to secondary+ cyclogenesis. A further explanation of this process is given in Appendix A.

As for Figures 6 and 7, this analysis was repeated for secondary+ cyclones passing through our regions at 45°N and 65°N and their preceding primary cyclones (Figures S6 and S7). Similar results are found with the dipole in stability anomalies closely following the jet axis and moving southward or northward for secondary+ cyclones impacting 45°N (Figure S6) and 65°N (Figure S7). The role of the jet anomalies in driving the latitude of the stability anomalies is clear, with the evolution of the anomalies with downstream propagation of the primary cyclone also apparent.

The relations identified in sections 3.2 and 3.3 are brought together, illustrated and summarized in Figure 9. In this figure it is shown how secondary+ cyclones passing through the different geographical regions (65°N, 55°N and 45°N) form close to the European continent, with their preceding primary cyclones forming over the Gulf Stream and near the coast of North America, with their lysis over the central North Atlantic. The occurrence of RWB on one or both sides of the jet affects the tilt of the jet in the exit region, which could be a result of the different baroclinic life cycles of the primary cyclones. The acceleration of the jet is then associated with an amplification of the stability dipole in a north–south direction across the jet, which likely further aids the cyclogenesis and intensification progress of secondary+ cyclones. Variations in these anomalies are then associated with changes in the genesis latitude and subsequent track of the secondary+ cyclones towards western Europe.

3.4 | Secondary+ cyclones and clustering over western Europe

In this section the importance of secondary+ cyclones for periods of clustering is investigated. The aim is to understand the relative impacts of secondary+ cyclogenesis and steering by the large-scale flow on the increase in the number of cyclones during these periods. Following Pinto *et al.* (2014) and Priestley *et al.* (2017b), clustering is defined as more than four cyclones in a 7-day period that
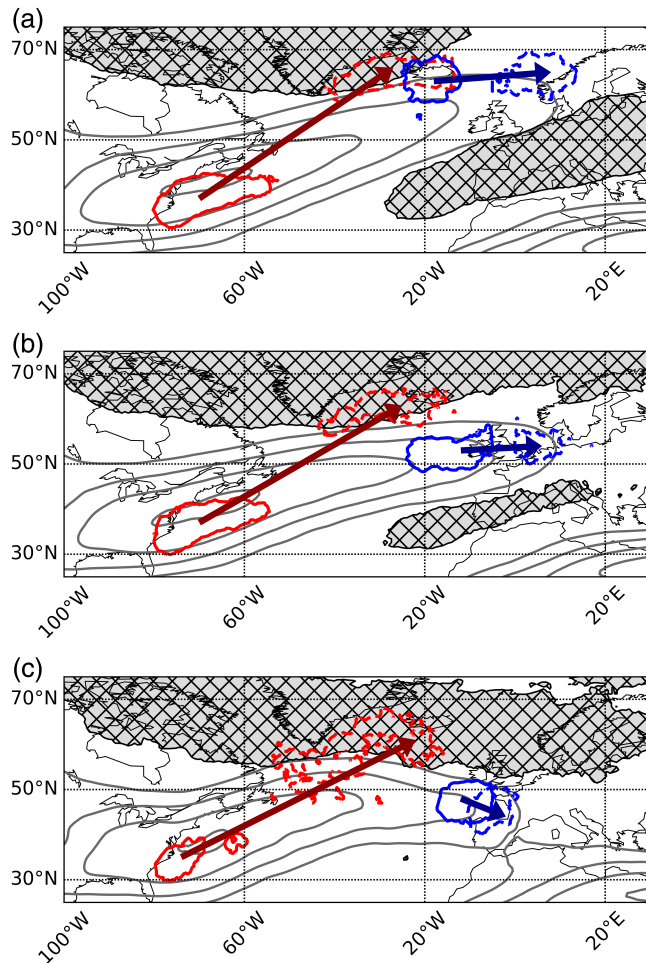
FIGURE 9 Summary figure illustrating the genesis (solid contours) and lysis (dashed contours) of primary cyclones (red) and their subsequent secondary+ cyclones (blue) that pass through the (a) 65°N, (b) 55°N and (c) 45°N regions. Also shown are contours of the 250 hPa wind speed (grey contours, every 5 m s⁻¹ above 30 m s⁻¹) and regions of RWB (grey hatching) averaged over the lifetimes of the secondary+ cyclones

pass through the 55°N region. The results are shown in Figure 10.

For all the cyclone classes shown in Figure 10, there is an increase in the number of cyclones in each class as cyclones pass through the 700-km 55°N region more frequently. However, the rate of increase is different for each of the classes. Firstly, the number of secondary+ cyclones (Figure 10a) increases almost linearly from less than one cyclone per 7 days for non-clustered periods to an average of four cyclones per 7 days during the most intensely clustered periods. A similar relationship is seen for solo cyclones (Figure 10b). There is on average one solo cyclone per 7 days in non-clustered periods, with a mean of around five cyclones per 7 days for the most clustered events. A different relationship is found for primary cyclones (Figure 10c). There is still an increase in the mean

number of primary cyclones as the intensity of clustering increases, but the total number is much lower. There are at most two primary cyclones per 7 days, with the average during non-clustered periods being ~0.2 cyclones per 7 days, and an average of ~1.5 cyclones per 7 days during the most clustered periods. This lower number of primary cyclones is to be expected from Figures 3b and 6g, as it is shown that primary cyclones rarely have a presence over western and northwestern Europe, which is especially the case for the 55°N cyclone families.

On average, secondary+ cyclones make up ~50% of all cyclones during severely clustered periods when more than ten cyclones are passing through the 55°N region in 1 week. From Figure 10 it is interesting to note the difference in the increase in the number of secondary+ and solo cyclones with intensity of clustering, compared to the lesser absolute increase in primary cyclones. This could be due to an increase in the cyclogenesis of secondary+ cyclones near the UK that could be assisted by the reduced stability environment associated with the development and propagation of the prior primary cyclone (Figure 8). This would result in more secondary+ cyclogenesis occurring and an increased contribution from cyclone families as the intensity of clustering increases. Alternatively, the amount of cyclogenesis may not be increasing, and the large-scale flow (Figure 7) may be much more dominant in steering all the cyclones along a similar track. This would lead to a large increase in the number of secondary+ cyclones with a minimal increase in the number of primary cyclones, as these rarely occur over western Europe.

To understand whether the dominant influence is due to an increase in cyclogenesis or the result of large-scale steering, the secondary+ cyclones that form in the North Atlantic during clustering periods (including 3 days prior, to allow for propagation across the UK) and those during non-clustered periods are investigated. The results are shown in Figure 11. Genesis densities of all secondary+ cyclones that form during clustered periods are shown in Figure 11a, with the anomaly relative to non-clustered periods shown in Figure 11c. During periods of clustering there is an increase in cyclogenesis over the UK and slightly to the west, with a decrease around the seas surrounding Greenland and Iceland and over the central North Atlantic. Both of these negative anomalies are regions that are commonly associated with secondary+ cyclogenesis (Figure 5c). It is also of interest to note that the relative number of cyclones forming per day across the entire North Atlantic Basin is higher for non-clustered days compared to clustered days.

There are also changes in secondary+ track density (Figure 11b,d), with an increase in the number of tracks over the UK by more than three cyclones per month. As
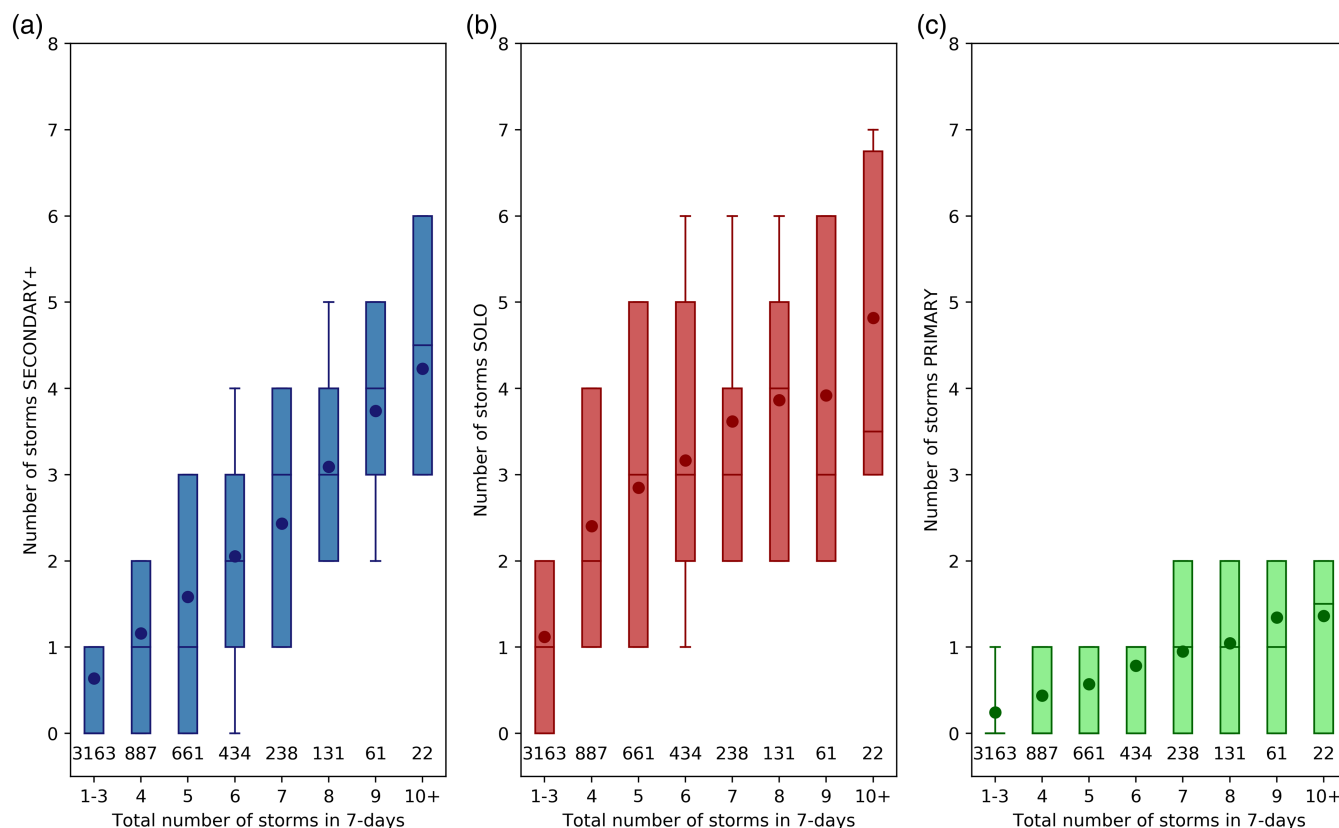
FIGURE 10 Number of secondary+ (a), solo (b) and primary (c) cyclones compared to the total number of cyclones passing through the 55°N region in a 7-day period. Boxes show the interquartile range, with the lines within the boxes representing the median and the dots showing the mean. Whiskers extend to the 20th and 80th percentiles. The numbers below each box represent the number of data points in that bin

for cyclogenesis, there is a decrease in track density in the region surrounding Greenland and Iceland. This shift south seen in the cyclogenesis density and track density (Figure 11c,d) is likely a result of the double-sided pattern of RWB associated with secondary+ cyclone propagation over the UK (Figure 7f), as well as the same pattern associated with periods of clustering (Priestley *et al.*, 2017b). This double-sided RWB pattern concentrates the formation of secondary+ cyclones further south than normal and over the region of low static stability (Figure 8f). The jet anomaly between the regions of RWB forces all cyclones to follow a similar track towards western Europe, as seen in Figure 11.

Changes in primary cyclogenesis and track density are shown in Figure 11e,f. Over the main cyclogenesis region of the Gulf Stream there are small changes in the rate of genesis of primary cyclogenesis during periods of clustering (Figure 11e), which is to be expected as these cyclones generally form regularly through baroclinic instability near the coast of North America (Mailier *et al.*, 2006). Cyclogenesis rate changes in the western North Atlantic do not exceed ±0.5 cyclones per month and rarely exceed ±0.15 cyclones per month for these primary

cyclones. There are very small increases in the rates of primary cyclogenesis over the eastern North Atlantic and the UK, but these are locally very small. There are pronounced differences in the track density of the primary cyclones (Figure 11f), with an extension and zonalization of the tracks over the UK leading to an increase of 1.5 cyclones per month. This anomaly is likely due to the enhanced upper-level flow associated with periods of clustering (Pinto *et al.*, 2014; Priestley *et al.*, 2017b), causing the cyclones to propagate further eastward than normal. This eastward propagation of the primary cyclones also helps to explain the negative anomalies in secondary+ cyclogenesis in the central North Atlantic (Figure 11c). As the primary cyclones are likely travelling downstream at a faster rate, the secondary+ cyclogenesis will be occurring further east than would normally be expected, resulting in a negative anomaly in the main cyclogenesis region, as seen in Figure 11c. Consistent with this is the fact that approximately 70% of the changes in the track density over the UK in Figure 11b,d are due to cyclones that form east of 40°W (not shown).

Furthermore, as with secondary+ cyclones there are similar changes in the genesis rates and track densities
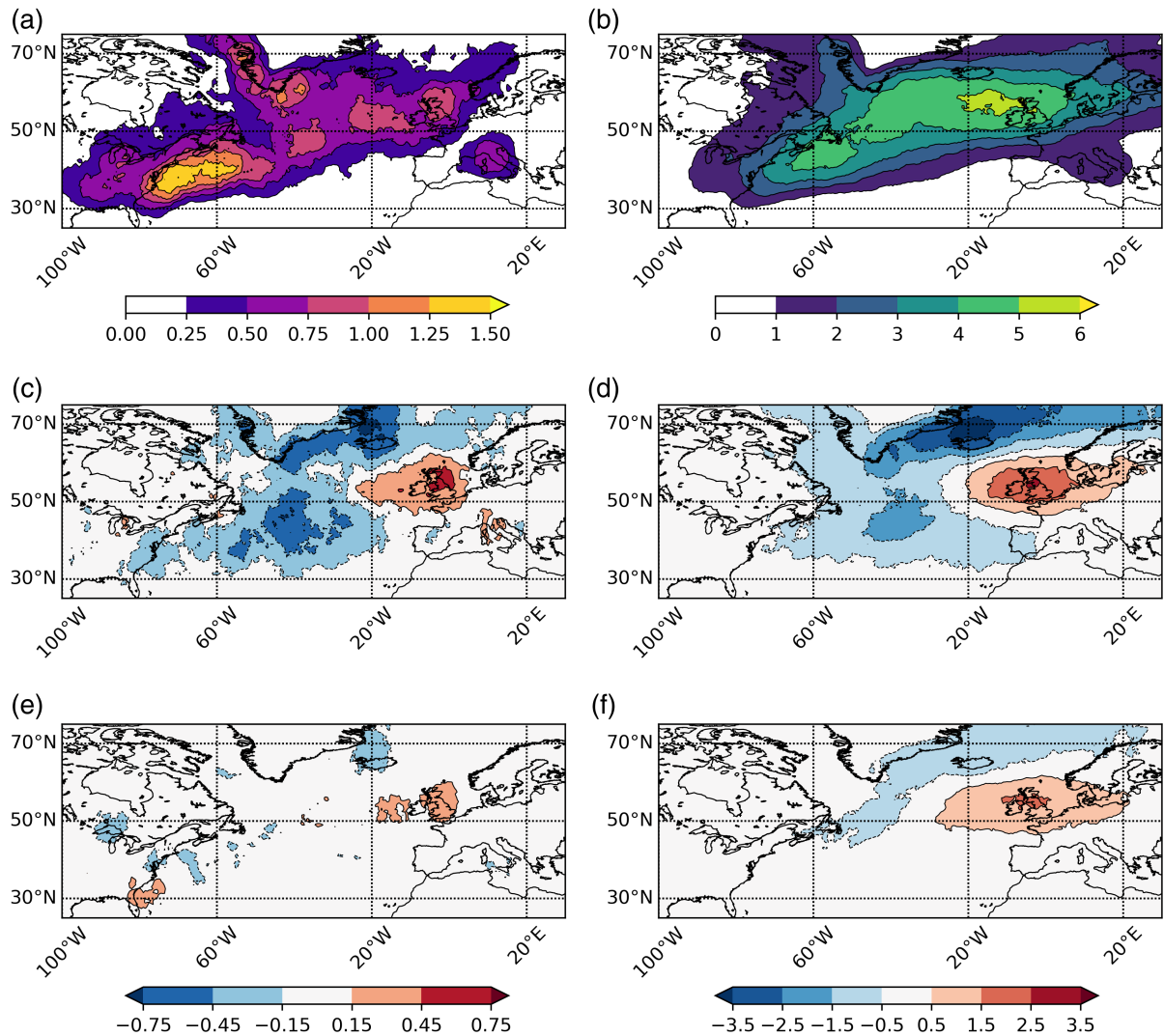
FIGURE 11 Genesis densities of secondary+ cyclones during clustered periods (a) and their respective track densities (b). Anomalies of (a) and (b) relative to non-clustered periods are shown in (c) and (d), respectively. The anomalies of primary cyclogenesis density and track density in clustered periods relative to non-clustered periods are shown in (e) and (f). In all panels, the unit is number of cyclones per 5° spherical cap per month

of solo cyclones (not shown) during clustered periods compared to non-clustered periods, albeit with less of a negative anomaly over the central North Atlantic, as this is not a common region for solo cyclogenesis.

This analysis thus shows that, as clustering becomes more intense, the number of secondary+ cyclones increases, with approximately 50% of cyclones being secondary+ cyclones during extreme periods of clustering. While there is an overall increase in the amount of secondary+ cyclogenesis near the UK, there is in fact a basin-wide reduction in the cyclogenesis rate and less cyclones present overall (in terms of the relative number per day) in the North Atlantic. This indicates that the large-scale environment redistributes secondary cyclones during periods of clustering rather than increasing the total number of secondary cyclones. The difference during

clustered periods is that those cyclones that do develop form preferentially close to western Europe, with this increase in the number of cyclones appearing to be driven by the dominant steering from the RWB and associated jet anomalies. This steering acts to concentrate all secondary+ cyclones that form to travel along a similar track, with changes in the frequency of RWB to the north and south of the jet affecting the jet angle and hence the genesis latitude and impact latitude of the secondary+ cyclones. In Walz *et al.* (2018), the variability of clustering near the UK was shown to be associated with the different phases of the NAO and the EA pattern, and the double-sided pattern of the RWB in Figure 7e,f has been shown to project onto the NAO (Messori and Caballero, 2015). Therefore, large-scale patterns such as the NAO and the EA pattern may play a role in modulating the

occurrence of secondary+ cyclones across the UK and other parts of western Europe.

4 | SUMMARY AND DISCUSSION

In this study, the occurrence of secondary+ cyclones and the cyclone families to which they belong, and how these phenomena contribute to the North Atlantic storm track, are investigated. Despite the comprehensive analysis of secondary cyclones by Schemm and Sprenger (2015) and Schemm *et al.* (2018), these authors did not objectively identify and compare the related primary cyclones, or quantify any differences in their preferential locations of genesis, track and lysis. To identify secondary+ cyclones and their associated primary cyclones the method of Schemm and Sprenger (2015) is followed and applied to the cyclone identification and tracking algorithm of Murray and Simmonds (1991). Three distinctly different cyclone classes are identified: primary, secondary+ and solo. The main results of this study are as follows.

- Primary and secondary+ cyclone classes make up more than 50% of all cyclones across the North Atlantic Ocean, and are therefore vital for the structure of the North Atlantic storm track. Primary cyclones tend to form over the Gulf Stream and are commonly found close to the coast of North America and the western North Atlantic Ocean. Secondary+ cyclones form over the Gulf Stream, but also over the central North Atlantic. Solo cyclones are most commonly found over continents, the Mediterranean and high latitudes of the North Atlantic. The preferential locations of the secondary+ cyclones across the central and eastern North Atlantic are a result of primary cyclones propagating in a northeasterly direction from where they form near the Gulf Stream, with secondary+ cyclones most likely forming on their southern flank.
- Primary cyclones are associated with the development of an environment that is favourable for secondary+ cyclone formation and downstream propagation towards Europe. Primary cyclone development is associated with an increase in RWB on one or both flanks of the jet, which is generally zonally extended and strengthened towards Europe. The enhanced jet is associated with a reduction in low-level static stability on the poleward flank of the jet, making the environment surrounding secondary+ cyclogenesis more favourable for cyclone formation and development around the left exit region of the jet.

- Secondary+ cyclones contribute approximately 50% of all cyclones during clustered periods. There is also an increase in the number of solo cyclones, with a smaller increase in the number of primary cyclones. The increase in the number of secondary+ cyclones during clustered periods is mainly a result of the influence of the large-scale flow that steers all cyclones along a similarly zonal path towards western Europe, as opposed to an overall increase in cyclogenesis. The presence of RWB acts to shift the latitude of cyclogenesis so that it is occurring at a similar latitude as the region impacted by the clustering.

As primary and secondary+ cyclones are most commonly found over the western and central/eastern sectors of the North Atlantic, it is clear that they are important for the overall structure of the North Atlantic storm track. The spatial separation of the two classes also illustrates the findings of Whittaker and Horn (1984) that individual cyclones rarely travel the entire length of the North Atlantic storm track, with those impacting Europe commonly forming very close to the continent (see also Hoskins and Hodges, 2002; Wernli and Schwierz, 2006; Dacre and Gray, 2009). The relative contributions of secondary+ cyclones in the central North Atlantic are higher in this study than those found by Schemm *et al.* (2018). These differences likely arise from differences in the cyclone identification and tracking schemes applied, with the Wernli and Schwierz (2006) method used in the aforementioned study commonly identifying only half as many cyclones as the Murray and Simmonds (1991) scheme used in this study (see fig. 2 in Pinto *et al.*, 2016). Furthermore, as the overall number of cyclones identified by the Wernli and Schwierz (2006) scheme is lower than the Murray and Simmonds (1991) scheme used in this study, it may be that the fractional number of cyclones contributing to periods of clustering is still consistent across the two methods. This would prove an interesting area for further exploration.

Primary and secondary+ cyclones follow different track orientations, with primary cyclones propagating more poleward and secondary+ cyclones having a more zonal nature to their track. For secondary+ cyclones impacting western Europe, their latitude of genesis is modulated by the presence of an anomalously strong jet and RWB, and secondary+ cyclones generally form in the left exit region of the extended upper-level jet. These jet and RWB anomalies are amplified with the downstream propagation of preceding primary cyclones. It may be the case that the differences in the jet/RWB responses to the primary cyclone are a result of differing baroclinic life cycles of primary cyclones (Thorncroft *et al.*, 1993) and

the differing momentum fluxes associated with the wave breaking from the two life cycles. Based on the jet/RWB pattern that is generated with the passage of these cyclones families over Europe, it could be hypothesized that the passages of these families in specific locations are associated with various phases of the NAO or EA pattern (see Messori and Caballero, 2015; Walz *et al.*, 2018), with the primary cyclones potentially playing a key role in modulating these large-scale patterns of variability on daily time-scales (Rivière and Orlanski, 2007; Gómara *et al.*, 2014b).

Secondary+ cyclones are also shown to form in regions of reduced low-level static stability, with the region of low stability dictated by the latitude of the jet exit. These findings are consistent with Schemm and Sprenger (2015), and also Wang and Rogers (2001) and Dacre and Gray (2009), who illustrated that cyclones forming in the eastern North Atlantic were more commonly associated with a lower-stability environment. It is likely that the reduced stability contributes to faster growth or deeper cyclones as opposed to additional genesis (Dacre and Gray, 2006). These results, coupled with the common genesis of cyclones in the eastern North Atlantic, provides further evidence for the hypothesis of Dacre and Gray (2009) that secondary+ cyclones are most closely aligned with Type C cyclogenesis. The cyclogenesis locations also suggest that our primary cyclones may be closely aligned with Type B cyclones, and solo cyclones to Type A cyclones. These classifications and their relations to the cyclone families could be quantified further using a quasi-geostrophic vertical velocity framework to distinguish the cyclone types (as in Deveson *et al.*, 2002; Plant *et al.*, 2003).

There are several limitations of this study. First, only one reanalysis product was utilized (ERA-Interim) with only 36 years of data. Future avenues of research could include investigating secondary cyclones in other reanalysis products, with the results from this study compared using consistent time periods from multiple products. In addition, only one cyclone identification and tracking algorithm has been used, with just one method for identifying synoptic-scale frontal features. Results have been shown to be sensitive to the choice of cyclone identification methodology, although most methods are consistent for mature phases of the cyclone life cycle, particularly for intense systems (Neu *et al.*, 2013). However, it would be of interest to compare the results of this study and that of Schemm and Sprenger (2015) with results from other identification schemes. Other frontal identification schemes are also available (e.g., Hewson, 1998; Simmonds *et al.*, 2012), and it would be of interest to compare our results to those from secondary+ cyclones identified using a different methodology.

Further research directions could also include an investigation into the process of frontal-wave cyclogenesis for other oceanic basins such as the Pacific, as this process also occurs in other geographical regions (Schemm *et al.*, 2018). In addition, a quantification of the role of the NAO or other leading atmospheric patterns in controlling the density of secondary+ cyclones would be of interest. Furthermore, given the database of cyclone types that has been created in this study, an examination of the physical differences (e.g., life cycle, intensity, deepening rate, structure, etc.) in the different classes would be of interest. Previous studies have shown differences in eastern and western North Atlantic cyclones and their evolution characteristics (e.g., Dacre and Gray, 2009; Čampa and Wernli, 2012), with the assumption that the two regional cyclone types are systematically different, and performing the same analysis for primary versus secondary+ cyclones would be an interesting addition to this analysis.

With regard to the results presented in this study, further in-depth analysis of the processes driving our secondary+ cyclones would be of interest, especially with the aim of building on the results of Schemm and Sprenger (2015) and investigating the role of the environment on specific cyclone features. It would be of particular interest to perform idealized mesoscale simulations of these cyclogenesis events to examine their sensitivity to atmospheric conditions. Evidence of simulated secondary+ cyclones has been demonstrated as an upstream response to the forcing of a primary cyclone via an upper-level PV anomaly in some idealized channel simulations (Schemm *et al.*, 2013). Furthermore, sensitivity experiments investigating drivers of the primary and secondary+ track orientation would also be an interesting avenue to pursue, with the upper-level PV structure and moist processes being shown to be important for the poleward propagation of idealized midlatitude cyclones (Coronel *et al.*, 2015). Finally, the superposition of the polar and subtropical jets has been shown to be important for some cyclogenesis events near the eastern coast of North America and in initiating a strengthening of the upper-level flow (Winters and Martin, 2017); it would therefore be of interest to explore how these superposition events affect the jet structure downstream and impact the formation of primary cyclones in the vicinity of the superpositions.

ORCID

Matthew D. K. Priestley https://orcid.org/0000-0002-5488-3959

Sebastian Schemm https://orcid.org/0000-0002-1601-5683

Joaquim G. Pinto https://orcid.org/0000-0002-8865-1769

REFERENCES

Adamson, D., Belcher, S.E., Hoskins, B.J. and Plant, R.S. (2006) Boundary-layer friction in midlatitude cyclones. *Quarterly Journal of the Royal Meteorological Society*, 132, 101–124.

Barnes, E.A. and Hartmann, D.L. (2012) Detection of Rossby wave breaking and its response to shifts of the midlatitude jet with climate change. *Journal of Geophysical Research: Atmospheres*, 117, D09117

Bell, G.D. and Bosart, L.F. (1989) The large-scale atmospheric structure accompanying New England coastal frontogenesis and associated North American east coast cyclogenesis. *Quarterly Journal of the Royal Meteorological Society*, 115, 1133–1146.

Berry, G., Reeder, M.J. and Jakob, C. (2011) A global climatology of atmospheric fronts. *Geophysical Research Letters*, 38, L04809

Bishop, C.H. and Thorpe, A.J. (1994a) Frontal wave stability during moist deformation frontogenesis. Part I. Linear wave dynamics. *Journal of the Atmospheric Sciences*, 51, 852–873.

Bishop, C.H. and Thorpe, A.J. (1994b) Frontal wave stability during moist deformation frontogenesis. Part II. The suppression of nonlinear wave development. *Journal of the Atmospheric Sciences*, 51, 874–888.

Bjerknes, J. and Solberg, H. (1922) Life cycle of cyclones and the polar front theory of atmospheric circulation. *Geophysisks Publikationer*, 3, 3–18.

Bosart, L.F. (1975) New England coastal frontogenesis. *Quarterly Journal of the Royal Meteorological Society*, 101, 957–978.

Brayshaw, D.J., Hoskins, B. and Blackburn, M. (2009) The basic ingredients of the North Atlantic storm track. Part I. Land–sea contrast and orography. *Journal of the Atmospheric Sciences*, 66, 2539–2558.

Brayshaw, D.J., Hoskins, B. and Blackburn, M. (2011) The basic ingredients of the North Atlantic storm track. Part II. Sea surface temperatures. *Journal of the Atmospheric Sciences*, 68, 1784–1805.

Čampa, J. and Wernli, H. (2012) A PV perspective on the vertical structure of mature midlatitude cyclones in the Northern Hemisphere. *Journal of the Atmospheric Sciences*, 69, 725–740.

Catto, J.L. and Pfahl, S. (2013) The importance of fronts for extreme precipitation. *Journal of Geophysical Research: Atmospheres*, 118, 10791–10801.

Chaboureau, J. and Thorpe, A.J. (1999) Frontogenesis and the development of secondary wave cyclones in FASTEX. *Quarterly Journal of the Royal Meteorological Society*, 125, 925–940.

Coronel, B., Ricard, D., Rivière, G. and Arbogast, P. (2015) Role of moist processes in the tracks of idealized midlatitude surface cyclones. *Journal of the Atmospheric Sciences*, 72, 2979–2996.

Dacre, H.F. and Gray, S.L. (2006) Life-cycle simulations of shallow frontal waves and the impact of deformation strain. *Quarterly Journal of the Royal Meteorological Society*, 132, 2171–2190.

Dacre, H.F. and Gray, S.L. (2009) The spatial distribution and evolution characteristics of North Atlantic cyclones. *Monthly Weather Review*, 137, 99–115.

Davis, C.A. and Emanuel, K.A. (1991) Potential vorticity diagnostics of cyclogenesis. *Monthly Weather Review*, 119, 1929–1953.

Dee, D., Uppala, S.M., Simmons, A.J., Berrisford, P., Poli, P., Kobayashi, S., Andrae, U., Balmaseda, M.A., Balsamo, G., Bauer, P., Bechtold, P., Beljaars, A.C.M., van de Berg, L., Bidlot, J., Bormann, N., Delson, C., Dragani, R., Fuentes, M., Geer, A.J., Haimberger, L., Healy, S.B., Hersbach, H., Hólm, E.V., Isaksen, L., Kållberg, P., Köhler, M., Matricardi, M., McNally, A.P., Monge-Sanz, B.M., Morcrette, J.-J., Park, B.-K., Peubey, C., de Rosnay, P., Tavolato, C., Thépaut, J.-N. and Vitart, F. (2011) The ERA-Interim reanalysis: configuration and performance of the data assimilation system. *Quarterly Journal of the Royal Meteorological Society*, 137, 553–597.

Deveson, A.C.L., Browning, K.A. and Hewson, T.D. (2002) A classification of FASTEX cyclones using a height-attributable quasi-geostrophic vertical-motion diagnostic. *Quarterly Journal of the Royal Meteorological Society*, 128, 93–117.

Economou, T., Stephenson, D.B., Pinto, J.G., Shaffrey, L.C. and Zappa, G. (2015) Serial clustering of extratropical cyclones in a multi-model ensemble of historical and future simulations. *Quarterly Journal of the Royal Meteorological Society*, 141, 3076–3087.

Flocas, H.A., Simmonds, I., Kouroutzoglou, J., Keay, K., Hatzaki, M., Bricolas, V. and Asimakopoulos, D. (2010) On cyclonic tracks over the eastern Mediterranean. *Journal of Climate*, 23, 5243–5257.

Gómara, I., Pinto, J.G., Woollings, T., Masato, G., Zurita-Gotor, P. and Rodríguez-Fonseca, B. (2014a) Rossby wave-breaking analysis of explosive cyclones in the Euro-Atlantic sector. *Quarterly Journal of the Royal Meteorological Society*, 140, 738–753.

Gómara, I., Rodríguez-Fonseca, B., Zurita-Gotor, P. and Pinto, J. (2014b) On the relation between explosive cyclones affecting Europe and the North Atlantic Oscillation. *Geophysical Research Letters*, 41, 2182–2190.

Gray, S.L. and Dacre, H.F. (2006) Classifying dynamical forcing mechanisms using a climatology of extratropical cyclones. *Quarterly Journal of the Royal Meteorological Society*, 132, 1119–1137.

Gyakum, J.R., Carrera, M., Zhang, D.-L., Miller, S., Caveen, J., Benoit, R., Black, T., Buzzi, A., Chouinard, C., Fantini, M., Folloni, C., Katzfey, J.J., Kuo, Y.-H., Lalaurette, F., Low-Nam, S., Mailhot, J., Malguzzi, P., McGregor, J.L., Nakamura, M., Tripoli, G. and Wilson, C. (1996) A regional model intercomparison using a case of explosive oceanic cyclogenesis. *Weather and Forecasting*, 11, 521–543.

Hanley, J. and Caballero, R. (2012) The role of large-scale atmospheric flow and Rossby wave breaking in the evolution of extreme windstorms over Europe. *Geophysical Research Letters*, 39, L21708

Hewson, T.D. (1998) Objective fronts. *Meteorological Applications*, 5, 37–65.

Hofstätter, M., Chimani, B., Lexer, A. and Blöschl, G. (2016) A new classification scheme of European cyclone tracks with relevance to precipitation. *Water Resources Research*, 52, 7086–7104.

Hope, P., Keay, K., Pook, M., Catto, J., Simmonds, I., Mills, G., McIntosh, P., Risbey, J. and Berry, G. (2014) A comparison of automated methods of front recognition for climate studies: a case study in southwest Western Australia. *Monthly Weather Review*, 142, 343–363.

Hoskins, B. and Berrisford, P. (1988) A potential vorticity perspective of the storm of 15–16 October 1987. *Weather*, 43, 122–129.

Hoskins, B.J. and Hodges, K.I. (2002) New perspectives on the Northern Hemisphere winter storm tracks. *Journal of the Atmospheric Sciences*, 59, 1041–1061.

Hoskins, B.J., McIntyre, M.E. and Robertson, A.W. (1985) On the use and significance of isentropic potential vorticity maps. *Quarterly Journal of the Royal Meteorological Society*, 111, 877–946.

Joly, A. and Thorpe, A.J. (1990) Frontal instability generated by tropospheric potential vorticity anomalies. *Quarterly Journal of the Royal Meteorological Society*, 116, 525–560.

Kuo, Y.-H., Gyakum, J.R. and Guo, Z. (1995) A case of rapid continental mesoscale cyclogenesis. Part I. Model sensitivity experiments. *Monthly Weather Review*, 123, 970–997.

Ludwig, P., Pinto, J.G., Hoepp, S.A., Fink, A.H. and Gray, S.L. (2015) Secondary cyclogenesis along an occluded front leading to damaging wind gusts: windstorm Kyrill, January 2007. *Monthly Weather Review*, 143, 1417–1437.

Mailier, P.J., Stephenson, D.B., Ferro, C.A.T. and Hodges, K.I. (2006) Serial clustering of extratropical cyclones. *Monthly Weather Review*, 134, 2224–2240.

Masato, G., Hoskins, B.J. and Woollings, T. (2013) Wave-breaking characteristics of Northern Hemisphere winter blocking: a two-dimensional approach. *Journal of Climate*, 26, 4535–4549.

Messori, G. and Caballero, R. (2015) On double Rossby wave breaking in the North Atlantic. *Journal of Geophysical Research: Atmospheres*, 120, 11129–11150.

Miller, J.E. (1946) Cyclogenesis in the Atlantic coastal region of the United States. *Journal of Meteorology*, 3, 31–44.

Murray, R.J. and Simmonds, I. (1991) A numerical scheme for tracking cyclone centres from digital data. Part I. Development and operation of the scheme. *Australian Meteorological Magazine*, 39, 155–166.

Neu, U., Akperov, M.G., Bellenbaum, N., Benestad, R., Blender, R., Caballero, R., Cocozza, A., Dacre, H.F., Feng, Y., Fraedrich, K., Grieger, J., Gulev, S., Hanley, J., Hewson, T., Inatsu, M., Keay, K., Kew, S.F., Kindem, I., Leckebusch, G.C., Liberato, M.L.R., Lionello, P., Mokhov, I.I., Pinto, J.G., Raible, C.C., Reale, M., Rudeva, I., Schuster, M., Simmonds, I., Sinclair, M., Sprenger, M., Tilinina, N.D., Trigo, I.F., Ulbrich, S., Ulbrich, U., Wang, X.L. and Wernli, H. (2013) IMILAST: a community effort to intercompare extratropical cyclone detection and tracking algorithms. *Bulletin of the American Meteorological Society*, 94, 529–547.

Nielsen, J.W. (1989) The formation of New England coastal fronts. *Monthly Weather Review*, 117, 1380–1401.

Papritz, L., Pfahl, S., Rudeva, I., Simmonds, I., Sodemann, H. and Wernli, H. (2014) The role of extratropical cyclones and fronts for Southern Ocean freshwater fluxes. *Journal of Climate*, 27, 6205–6224.

Parker, D.J. (1998) Secondary frontal waves in the North Atlantic region: a dynamical perspective of current ideas. *Quarterly Journal of the Royal Meteorological Society*, 124, 829–856.

Pearce, R., Lloyd, D. and McConnell, D. (2001) The post-Christmas 'French' storms of 1999. *Weather*, 56, 81–91.

Petterssen, S., Dunn, G.E. and Means, L.L. (1955) Report of an experiment in forecasting of cyclone development. *Journal of Meteorology*, 12, 58–67.

Pinto, J.G., Gómara, I., Masato, G., Dacre, H.F., Woollings, T. and Caballero, R. (2014) Large-scale dynamics associated with clustering of extratropical cyclones affecting Western Europe. *Journal of Geophysical Research: Atmospheres*, 119, 13704–13719.

Pinto, J.G., Spangehl, T., Ulbrich, U. and Speth, P. (2005) Sensitivities of a cyclone detection and tracking algorithm: individual tracks and climatology. *Meteorologische Zeitschrift*, 14, 823–838.

Pinto, J.G., Ulbrich, S., Economou, T., Stephenson, D.B., Karremann, M.K. and Shaffrey, L.C. (2016) Robustness of serial clustering of extratropical cyclones to the choice of tracking method. *Tellus A*, 68, 32204

Pinto, J.G., Zacharias, S., Fink, A.H., Leckebusch, G.C. and Ulbrich, U. (2009) Factors contributing to the development of extreme North Atlantic cyclones and their relationship with the NAO. *Climate Dynamics*, 32, 711–737.

Plant, R., Craig, G.C. and Gray, S. (2003) On a threefold classification of extratropical cyclogenesis. *Quarterly Journal of the Royal Meteorological Society*, 129, 2989–3012.

Priestley, M.D.K., Pinto, J.G., Dacre, H.F. and Shaffrey, L.C. (2017a) The role of cyclone clustering during the stormy winter of 2013/2014. *Weather*, 72, 187–192.

Priestley, M.D.K., Pinto, J.G., Dacre, H.F. and Shaffrey, L.C. (2017b) Rossby wave breaking, the upper level jet, and serial clustering of extratropical cyclones in western Europe. *Geophysical Research Letters*, 44, 514–521.

Raible, C.C., Della-Marta, P.M., Schwierz, C., Wernli, H. and Blender, R. (2008) Northern Hemisphere extratropical cyclones: a comparison of detection and tracking methods and different reanalyses. *Monthly Weather Review*, 136, 880–897.

Rivals, H., Cammas, J.-P. and Renfrew, I.A. (1998) Secondary cyclogenesis: the initiation phase of a frontal wave observed over the eastern Atlantic. *Quarterly Journal of the Royal Meteorological Society*, 124, 243–268.

Rivière, G. and Joly, A. (2006a) Role of the low-frequency deformation field on the explosive growth of extratropical cyclones at the jet exit. Part I. Barotropic critical region. *Journal of the Atmospheric Sciences*, 63, 1965–1981.

Rivière, G. and Joly, A. (2006b) Role of the low-frequency deformation field on the explosive growth of extratropical cyclones at the jet exit. Part II. Baroclinic critical region. *Journal of the Atmospheric Sciences*, 63, 1982–1995.

Rivière, G. and Orlanski, I. (2007) Characteristics of the Atlantic storm-track eddy activity and its relation with the North Atlantic Oscillation. *Journal of the Atmospheric Sciences*, 64, 241–266.

Schemm, S., Rudeva, I. and Simmonds, I. (2015) Extratropical fronts in the lower troposphere – global perspectives obtained from two automated methods. *Quarterly Journal of the Royal Meteorological Society*, 141, 1686–1698.

Schemm, S. and Sprenger, M. (2015) Frontal-wave cyclogenesis in the North Atlantic – a climatological characterisation. *Quarterly Journal of the Royal Meteorological Society*, 141, 2989–3005.

Schemm, S., Sprenger, M. and Wernli, H. (2018) When during their life cycle are extratropical cyclones attended by fronts?. *Bulletin of the American Meteorological Society*, 99, 149–165.

Schemm, S., Wernli, H. and Papritz, L. (2013) Warm conveyor belts in idealized moist baroclinic wave simulations. *Journal of the Atmospheric Sciences*, 70, 627–652.

Schär, C. and Davies, H.C. (1990) An instability of mature cold fronts. *Journal of the Atmospheric Sciences*, 47, 929–950.

Simmonds, I., Keay, K. and Bye, J.A.T. (2012) Identification and climatology of Southern Hemisphere mobile fronts in a modern reanalysis. *Journal of Climate*, 25, 1945–1962.

Thomas, C.M. and Schultz, D.M. (2019) What are the best thermodynamic quantity and function to define a front in gridded model output?. *Bulletin of the American Meteorological Society*, 100, 873–895.

Thorncroft, C.D., Hoskins, B.J. and McIntyre, M.E. (1993) Two paradigms of baroclinic-wave life-cycle behaviour. *Quarterly Journal of the Royal Meteorological Society*, 119, 17–55.

Uccellini, L.W., Petersen, R.A., Kocin, P.J., Brill, K.F. and Tuccillo, J.J. (1987) Synergistic interactions between an upper-level jet streak and diabatic processes that influence the development of a low-level jet and a secondary coastal cyclone. *Monthly Weather Review*, 115, 2227–2261.

Vitolo, R., Stephenson, D.B., Cook, L.M. and Mitchell-Wallace, K. (2009) Serial clustering of intense European storms. *Meteorologische Zeitschrift*, 18, 411–424.

Walz, M.A., Befort, D.J., Kirchner-Bossi, N.O., Ulbrich, U. and Leckebusch, G.C. (2018) Modelling serial clustering and inter-annual variability of European winter windstorms based on large-scale drivers. *International Journal of Climatology*, 38, 3044–3057.

Wang, C.-C. and Rogers, J.C. (2001) A composite study of explosive cyclogenesis in different sectors of the North Atlantic. Part I. Cyclone structure and evolution. *Monthly Weather Review*, 129, 1481–1499.

Wernli, H., Dirren, S., Liniger, M.A. and Zillig, M. (2002) Dynamical aspects of the life cycle of the winter storm 'Lothar' (24–26 December 1999). *Quarterly Journal of the Royal Meteorological Society*, 128, 405–429.

Wernli, H. and Schwierz, C. (2006) Surface cyclones in the ERA-40 dataset (1958–2001). Part I. Novel identification method and global climatology. *Journal of the Atmospheric Sciences*, 63, 2486–2507.

Whittaker, L.M. and Horn, L.H. (1984) Northern Hemisphere extratropical cyclone activity for four mid-season months. *Journal of Climatology*, 4, 297–310.

Winters, A.C. and Martin, J.E. (2017) Diagnosis of a North American polar–subtropical jet superposition employing piecewise potential vorticity inversion. *Monthly Weather Review*, 145, 1853–1873.

APPENDIX A: CHANGES IN STATIC STABILITY BASED ON THERMAL WIND BALANCE

Thermal wind balance formulated in terms of potential temperature (θ) in pressure (p) coordinates can be expressed as follows:

$$\frac{\partial u}{\partial p} = -\frac{1}{f \rho \theta} \left(\frac{\partial \theta}{\partial y} \right)_p. \tag{A1}$$

Equation A1 can be simplified further by treating the Coriolis parameter (f), density (ρ) and the potential temperature (θ) as constant, thereby giving
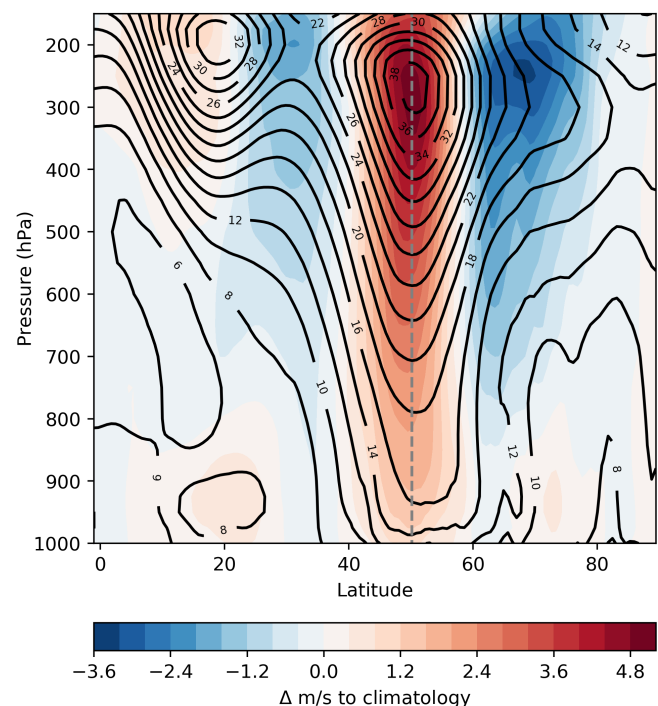
$$\frac{\partial u}{\partial p} \approx -\left(\frac{\partial \theta}{\partial y} \right)_p. \tag{A2}$$

In Equation 1, the low-level static stability is formulated in pressure coordinates. By treating p, g, R, T and $\overline{\theta}$ as approximately constant, this can be expressed as

$$N^2 \approx \frac{\partial \theta}{\partial p}. \tag{A3}$$

Through differentiating Equation A2 with respect to p, the following relationship is obtained:

$$\frac{\partial^2 u}{\partial p^2} \approx -\frac{\partial}{\partial p} \left(\frac{\partial \theta}{\partial y} \right)_p \approx -\frac{\partial^2 u}{\partial p \partial y} \approx -\frac{\partial}{\partial y} \left(\frac{\partial \theta}{\partial p} \right). \tag{A4}$$

FIGURE A1 Composite image of zonal mean wind at the time of secondary+ cyclogenesis for secondary+ cyclones passing through 55°N. Zonal mean from 40–0°W. Black contours are the full field at the time of cyclogenesis and the coloured filled contours are the anomalies relative to the long-term climatology in m·s⁻¹. The grey dashed line represents the midlatitude jet axis
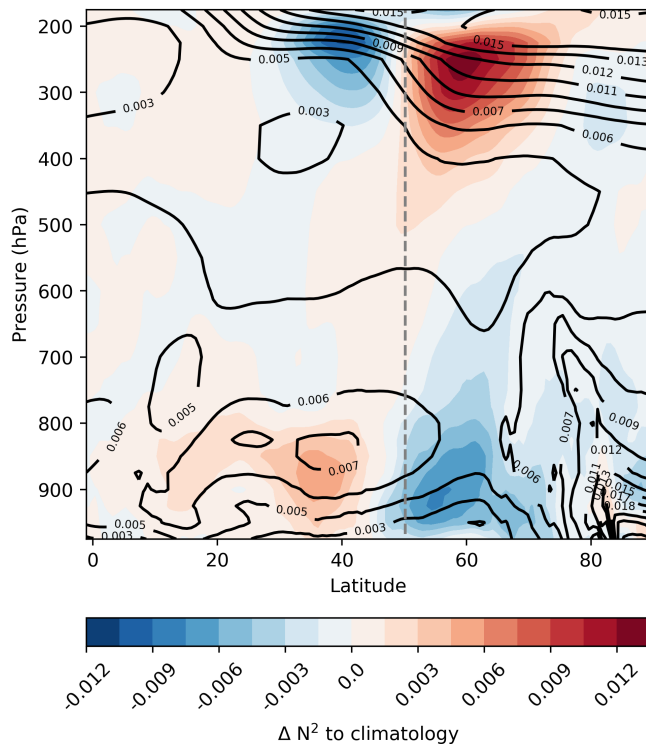
FIGURE A2 Composite image of zonal mean static stability (N^2) at the time of secondary+ cyclogenesis for secondary+ cyclones passing through 55°N. Zonal mean from 40–0°W. Black contours are the full field at the time of cyclogenesis and the coloured filled contours are the anomalies relative to the long-term climatology. The grey dashed line represents the midlatitude jet axis

Using the relationship in Equation A3 substituted into Equation A4, it can therefore be stated that as the second derivative of u with respect to p increases, the meridional gradient of the static stability will become more negative.

From Figure 12 it can be seen that the anomalies in the jet are present throughout the depth of the atmosphere

with a peak between 200 and 350 hPa. These changes in jet speed with height imply that the value of $\partial u/\partial p$ will be positive below the jet maximum, have a value of zero at the height of the jet core and be negative above it. The maxima in $\partial u/\partial p$ will subsequently be in the middle troposphere. Through Equation A2 we can see that the gradient of θ will increase across the jet from south to north.

As $\partial u/\partial p$ will have a positive gradient in the lower troposphere and a negative gradient in the upper troposphere, through Equation A4 we learn that $\partial^2 u/\partial p^2$ will be positive in the lower troposphere, negative in the upper troposphere and have its minimum at the height of the jet maximum. The large values of $\partial^2 u/\partial p^2$ in the lower troposphere relate to a strong negative meridional N^2 (through Equation A4) and the large negative values at the height of the jet maximum result in a positive meridional gradient of N^2 at that height. These patterns are seen in Figure 13, with the stability gradients across the jet peaking at lower and upper levels, with negative N^2 anomalies on the poleward flank of the jet below 800 hPa. Furthermore, the anomalies of N^2 in the upper troposphere can be related to the large-scale RWB and the associated PV anomalies. The RWB on the poleward (equatorward) flank of the jet will be associated with positive (negative) PV anomalies. The positive (negative) PV anomalies are therefore related to positive (negative) anomalies of static stability within the anomaly itself due to the associated bending of the isentropes.

SUPPORTING INFORMATION

Additional Supporting Information may be found online in the supporting information tab for this article.